



EUMETSAT

ROM SAF

RADIO OCCULTATION METEOROLOGY

ROM SAF CDOP-2

Visiting Scientist Report 33:

**Assessment of Differences Between ROM SAF GRAS
Derived Brightness Temperatures and Hyperspectral
Infrared Brightness Temperature Observations**

Michelle Feltz

Danish Meteorological Institute (DMI)
European Centre for Medium-Range Weather Forecasts (ECMWF)
Institut d'Estudis Espacials de Catalunya (IEEC)
Met Office (METO)

DOCUMENT AUTHOR TABLE

	<i>Author(s)</i>	<i>Function</i>	<i>Date</i>	<i>Comment</i>
Prepared by:	Michelle Feltz	ROM SAF Visiting Scientist	30/10/2017	
Reviewed by (internal):	Johannes K. Nielsen	ROM SAF Scientist	17/08/2017	
Approved by:	Kent B. Lauritsen	ROM SAF Project Manager	30/10/2017	

DOCUMENT CHANGE RECORD

<i>Issue/Revision</i>	<i>Date</i>	<i>By</i>	<i>Description</i>
Draft 1	24/07/2017	MF	First draft
Draft 2	30/10/2017	MF	Changed figures 6.2-3,5,6,7,8,9 and text after review of JKN (17/08/2017); Revised text; Correct Eqn. 3-4, update figures (after discussions with JKN)
1.0	30/10/2017	JKN	Finalized version

DOCUMENT DISTRIBUTION LIST

The VS report is made available at the ROM SAF website.

VS AUTHOR AND DURATION

VS Author

This VS study was carried out by Ms. Michelle Feltz, University of Wisconsin – Madison, Madison, WI, USA; Email: michelle.feltz@ssec.wisc.edu

VS Duration

The VS study was performed during May – August 2017 at the University of Wisconsin – Madison with a one month visit to DMI, Copenhagen, Denmark during June 2017.

ROM SAF

The Radio Occultation Meteorology Satellite Application Facility (ROM SAF) is a decentralised processing center under EUMETSAT which is responsible for operational processing of GRAS radio occultation (RO) data from the Metop satellites and radio occultation data from other missions. The ROM SAF delivers bending angle, refractivity, temperature, pressure, humidity, and other geophysical variables in near-real time for NWP users, as well as reprocessed data (Climate Data Records) and offline data for users requiring a higher degree of homogeneity of the RO data sets. The reprocessed and offline data are further processed into globally gridded monthly-mean data for use in climate monitoring and climate science applications.

The ROM SAF also maintains the Radio Occultation Processing Package (ROPP) which contains software modules that aids users wishing to process, quality-control and assimilate radio occultation data from any radio occultation mission into NWP and other models.

The ROM SAF Leading Entity is the Danish Meteorological Institute (DMI), with Cooperating Entities: i) European Centre for Medium-Range Weather Forecasts (ECMWF) in Reading, United Kingdom, ii) Institut D'Estudis Espacials de Catalunya (IEEC) in Barcelona, Spain, and iii) Met Office in Exeter, United Kingdom. To get access to our products or to read more about the ROM SAF please go to: <http://www.romsaf.org>

Intellectual Property Rights

All intellectual property rights of the ROM SAF products belong to EUMETSAT. The use of these products is granted to every interested user, free of charge. If you wish to use these products, EUMETSAT's copyright credit must be shown by displaying the words "copyright (year) EUMETSAT" on each of the products used.

List of Contents

EXECUTIVE SUMMARY	5
1. INTRODUCTION	7
1.1 PURPOSE OF DOCUMENT.....	7
1.2 BACKGROUND	7
2. DATA AND RADIATIVE TRANSFER MODEL	9
2.1 RADIO OCCULTATION	9
2.2 HYPERSPECTRAL INFRARED SOUNDER.....	9
2.3 RADIATIVE TRANSFER MODEL INPUT.....	9
2.4 RADIATIVE TRANSFER MODEL.....	9
3. MATCHUP SCHEME	10
4. RADIATIVE TRANSFER CALCULATIONS	12
5. UNCERTAINTY ANALYSIS	16
5.1 RTM MODEL ERRORS	16
5.2 IR OBSERVATIONS.....	16
5.3 RO EXTRAPOLATION ERRORS	16
5.4 RO TEMPERATURE.....	19
5.5 TOTAL UNCERTAINTY	23
6. IR AND RO BT COMPARISONS	24
6.1 METHODS	24
6.2 RESULTS.....	24
6.2.1 <i>Seasonal</i>	24
6.2.2 <i>Monthly Time Series</i>	34
6.2.3 <i>Solar Zenith Angle Dependence</i>	36
7. CONCLUSIONS	39
7.1 SUMMARY	39
7.2 RECOMMENDATIONS	40
7.3 ACKNOWLEDGMENTS.....	41
8. APPENDIX	42
8.1 BT CALCULATION SENSITIVITY STUDY.....	42
8.1.1 <i>Constant Emissivity</i>	42
REFERENCES	43
LIST OF ACRONYMS	46

Executive Summary

This activity demonstrated a comparison of RO temperature products to hyperspectral IR sounder observations in brightness temperature space with the goals of:

- 1] assessing possible differences between hyperspectral infrared brightness temperature measurements and calculated brightness temperatures from GPS radio occultation measurements, and
- 2] improving contact between RO and IR communities.

This study made use of EUMETSAT IASI and NASA CrIS radiance measurements in addition to ROM SAF GRAS temperature products from both the Metop-A and Metop-B satellites. Strict collocation requirements were applied to the data over the two years of 2015 through 2016 to obtain spatiotemporally coincident measurements from IASI-A/GRAS-A, IASI-B/GRAS-B, CrIS/GRAS-A, and CrIS/GRAS-B. Infrared radiative transfer calculations were then performed using the Optimal Spectral Sampling RTM for the 15 micron absorption region with the motivation for assessing differences within the upper-troposphere, lower-stratosphere temperature. Brightness temperatures were computed using the collocated GRAS temperature products, including “dry” temperature (zero humidity assumed), “wet” temperature (ERA-Interim forecast used as background for retrieval), and background temperature (ERA-Interim analysis). A total BT uncertainty estimate which included contributions from the IR measurements, RTM calculations, RO temperature extrapolation, and ROM SAF GRAS error products was compared to the calculated minus observed BT difference standard deviations, and was based upon single-sample, stochastic errors.

Seasonal and monthly, zonal results revealed consistency between the calculated minus observed BT difference biases corresponding to the four different collocation datasets, with differences between them being typically under ~ 0.25 K. The wet and background calculated minus observed BT difference biases were very similar, which could perhaps be an outcome of the high vertical resolution nature of the wet minus background temperature differences and the wide vertical layers which the IR radiative transfer smooths over. Seasonal variations of the bias existed in the extra-tropics and increased poleward. The dry BT bias varied more than the wet and background biases over time, having negative minima around summer solstices and positive maxima during winter solstices, being larger at upper levels around 20 hPa. An investigation of the difference bias dependence on solar zenith angle in the upper middle and lower stratosphere revealed three primary things: 1] a lack of dependence in the tropics, 2] an increase in the bias from negative to positive with solar zenith angle increasing over the ~ 40 - 130 degree range at the poles so that the GRAS BTs were warmer than the IR observations at night, and 3] that the dry bias was more similar to the wet and background biases for solar zenith angles larger than 90 degrees at the poles. Results for CrIS and IASI were qualitatively consistent, suggesting that these characteristics of the biases are globally representative, rather than simply representing characteristics for the local sampling times of the IR sounder platforms. Standard deviations of the calculated minus observed BTs were qualitatively similar across the matchup datasets as well.

General agreement of the background/wet standard deviation with the BT uncertainty existed in mid-latitude and polar winter regions, while polar summers had smaller than

expected background/wet standard deviations and tropical regions had slightly larger than expected standard deviations. The dry standard deviations were larger than the BT uncertainty in all zones for channels with main contributions from pressure levels above (in altitude) the ~70 hPa level, indicating that the total, dry BT uncertainty does not sufficiently account for the stochastic error sources. This was also seen in channels with contributions from pressure levels closer to the surface (100-300 hPa) in the JJA Antarctic zones.

Recommendations include the investigation of regions which showed disagreements between the calculated minus observed BT standard deviations and the total BT uncertainty estimate. This includes the upper stratosphere (~70-10 hPa) in all zones for the dry temperature, and it includes the polar summer and tropics for the wet/background temperature. Regions of relatively increased biases—specifically the polar regions around solstices and the lower stratospheric tropical region channels should also be investigated. Challenges in both the IR radiative transfer scheme and RO temperature derivation should be considered. Continued collaboration between the hyperspectral IR sounder and radio occultation communities could provide fruitful insights for both communities.

1. Introduction

1.1 Purpose of Document

This document contains the results from the ROM SAF Visiting Scientist activity VS33 with the objectives to:

- 1) assess possible differences between hyperspectral infrared brightness temperature measurements and calculated brightness temperatures from GPS radio occultation measurements, and discuss possible mutual benefits from combining data from different instruments on the Metop satellites for Near Real Time validation, and
- 2) improve contact between RO and IR communities.

The document is organized as follows: Chapter 2 describes the data and RTM that are used in the study, Chapter 3 and 4 describe the RO profile to IR radiance matchup application and RTM calculations respectively, Chapter 5 discusses the calculated BT uncertainty analysis used to define agreement between the IR observations and RO calculations, Chapter 6 shows the results of the IR observed and RO calculated BT comparison, and Chapter 7 contains conclusions.

1.2 Background

One of the available applications of GPS-RO is to aid radiometer retrievals of temperature with validation, and in some cases calibration, studies. Some efforts have been done previously in this direction within the ROM SAF. A VS study by Florian Ladstädter [Ladstädter, 2012] which compares brightness temperatures concludes that Metop A RO data are sufficiently accurate for use in calibrating Metop-A AMSU measurements independently of NWP (ECMWF) data. This study also revealed, however, that the “optimization” of bending angles at high altitudes has to be considered carefully. In the Continued Development and Operational Phase 3 (CDOP-3) a work package (WP 2410, Synthetic Brightness Temperature) has been scheduled to follow up on these findings by development of a Microwave Brightness temperature product for climate studies and instrument calibration. GPS-RO has previously been used for cross validation and assessment of infrared and microwave measurements and derived products [Yunck *et al.*, 2009; Divakarla *et al.*, 2014; Shi *et al.*, 2016; Feltz *et al.*, 2014a/b; Chou *et al.*, 2009; Isoz *et al.*, 2015], and has been used in experiments with “synergetic” products [e.g. Liu *et al.*, 2016, Ho *et al.*, 2007], yet no studies have yet been published on the comparison of hyperspectral infrared radiance measurements to forward propagated RO infrared radiances. While CDOP-3 WP 2410 is targeted at AMSU/MSU channels, this VS33 study complements the CDOP-3 development by addressing high spectral density infrared channels belonging to IASI and CrIS. Since GRAS shares platforms with IASI but not with CrIS, there are more collocations with IASI than CrIS—over 6500 per month globally for IASI and approximately 2000 for CrIS for matchups with minimal collocation errors (Feltz 2014c).

The aim of this study is to compare brightness temperatures observed by hyperspectral infrared sounders to brightness temperatures calculated using RO temperature products. With such statistical comparisons, either the high accuracy infrared measurements [Tobin,

2013] could be leveraged to provide an error assessment of the Metop-A and -B RO temperature products for various vertical regions of the atmosphere, or the RO could be used as a potential aid in calibration and accuracy assessment of the infrared measurements. In addition, the background temperature profiles used in 1D-Var are analyzed to assess whether the 1D-Var retrieval fits the radiances closer than the background. Specifically, the 15 micron carbon dioxide absorption region channels are assessed, which have weighting functions that are essentially contained within 200 hPa to 10 hPa vertical region. This allows for a focus on the lower stratospheric levels of the atmosphere. Simulations of RO Top Of Atmosphere (TOA) IASI and CrIS radiances are performed using the Optimal Spectral Sampling (OSS) infrared radiative transfer model [Moncet *et al.*, 2008]. The OSS model, produced by Atmospheric & Environmental Research Radiative Transfer Working Group, is a fast model based on the Line-by-Line Radiative Transfer Model. To define agreement between the IR observations and RO calculations, an estimated calculated BT uncertainty is calculated and accounts for contributions from multiple sources. For this, 1D-Var and background error profiles are calculated in radiance space with the aid of the OSS temperature Jacobian, and zonally representative dry temperature errors are estimated.

2. Data and Radiative Transfer Model

2.1 Radio Occultation

Radio occultation data is obtained through EUMETSAT's Radio Occultation Meteorology Satellite Application Facility (ROM SAF) (<http://www.romsaf.org>). The data product used for the present study is the CDR version 1.0-beta release, processed with software version GPAC 2.3.0.1. Dry, wet, and background temperature profile products from the GRAS instruments aboard Metop-A and Metop-B (referred to as GRAS -A and GRAS -B respectively) are used. The background profiles used in the 1D-Var calculations are defined by the ERA Interim forecast. Dry temperatures are defined on 247 levels while wet and background temperatures are defined on 60 model levels. Quality control of the RO products is performed on each individual profile during the processing and summarized in the 'PCD_summary' bit. For the user quality control consists in excluding profiles for which the 'pcd' variable is odd, which has been done in this study.

2.2 Hyperspectral Infrared Sounder

Hyperspectral infrared radiances from both EUMETSAT's IASI [Hilton *et al.*, 2012; Klaes *et al.*, 2007] and the JPSS Suomi-NPP CrIS [Han *et al.*, 2013; Tobin *et al.*, 2013; Strow *et al.*, 2013; Goldberg *et al.*, 2013] sounders are used. IASI radiances from Metop-A and Metop-B platforms (referred to as IASI-A and IASI-B respectively) are obtained through EUMETSAT from the IASI GDS Level 1C files (<http://archive.eumetsat.int/usc/>). The general quality flag, 'GQisFlagQual' is used to quality control the data—spectra with this variable set to 1 are excluded from analyses. NASA CrIS L1B radiances are obtained through NASA through the Suomi-NPP Sounder SIPS at the Jet Propulsion Laboratory and GES DISC. Only CrIS radiances for which the 'geo_quality' and '11b_quality' flags indicate no critical issues (i.e. are set to 0) are used.

2.3 Radiative Transfer Model Input

Carbon dioxide (CO₂) data is obtained from CarbonTracker (CT), NOAA's Earth System Research Laboratory CO₂ measurement and modeling system [Peters *et al.*, 2007]. Version CT2015, available for 2000-2014 as global 3x2° gridded monthly CO₂ mole fractions, is used (<http://carbontracker.noaa.gov>). Carbon dioxide estimates on the 3x2° monthly grid for the years 2015 through 2016 are obtained by extrapolation. Ozone, skin temperature, water vapor, and surface pressure are obtained from ECMWF's ERA-Interim reanalysis model which is run on 6 hourly increments (<http://www.ecmwf.int/en/research/climate-reanalysis/era-interim>) [Dee *et al.*, 2011]. The 0.75° gridded model level product has resolution equivalent to ~80 km and is available up to ~0.1 hPa.

2.4 Radiative Transfer Model

This study makes use of the Optimal Spectral Sampling (OSS) fast radiative transfer model (RTM). OSS has an accuracy of 0.05 K brightness temperature with respect to a reference line-by-line model [Moncet *et al.*, 2008, 2015] and is able to output infrared radiances and temperature Jacobians on CrIS and IASI's spectral resolutions.

3. Matchup Scheme

Matchup datasets for each of the IASI and CrIS radiance sets to GRAS temperatures are found for the years 2015 through 2016. The IASI and GRAS matchups are found for similar platforms, i.e. IASI-A to GRAS-A and IASI-B to GRAS-B, and there are four resulting matchup datasets. Temporal mismatch is minimized through the use of time restrictions on the IR measurement minus RO profiles times – \pm one hour is used for the CrIS and GRAS matchups to allow for a sufficient number of samples, and a -15 to 10 minute restriction is applied to the IASI and GRAS matchups to include a smaller, more manageable number of matchups which include an equal number of matchup GRAS occultations that are located on either side of the Metop platforms (i.e. GRAS measurements which are taken before or after the IASI measurements in time).

Spatial mismatch of the IR and RO data is minimized through the use a spatial collocation technique which accounts for each RO profiles' unique geometry. Specifically, the IR sounder field of regards, or measurement footprints, which are closest to the RO profile's latitude and longitude at various pressure levels are found—this results in sets of radiances which have different pressure levels 'assigned' to them. Then for each IR channel, the radiance set whose pressure level is closest to the channels temperature Jacobian maximum is selected for use. Using this method, matchup radiances for different channels are represented by measurements taken at different latitudes and longitudes based upon the RO profile geometry. Figure 3.1 illustrates an example of a 'radiance profile' for a single channel from an IASI-A and GRAS-A matchup case which traces the RO profile shape.

Examples of the GRAS to CrIS and IASI matchup datasets spatiotemporal sampling are shown in Figure 3.2. The difference between the equatorial crossing times of the GRAS Metop and CrIS SNPP platforms is reflected in the latitudinal distributions of the GRAS to IASI and CrIS matchups. Fewer number of samples are obtained for the CrIS/GRAS matchups in comparison to the IASI/GRAS matchups overall, with essentially no matchups occurring in the Tropics. Color of the markers depicts the solar zenith angle and suggests that different latitude regions can be characterized by specific solar zenith angles.

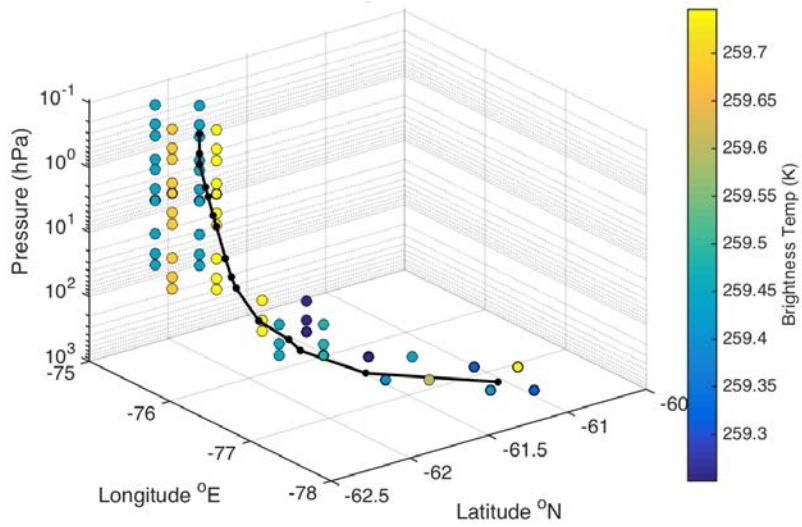


Figure 3.1. Illustration of an example IASI observed BT ‘profile’ (colored dots) for the 667.5 cm^{-1} channel shaded by Kelvin for a single GRAS profile (location depicted by black line).

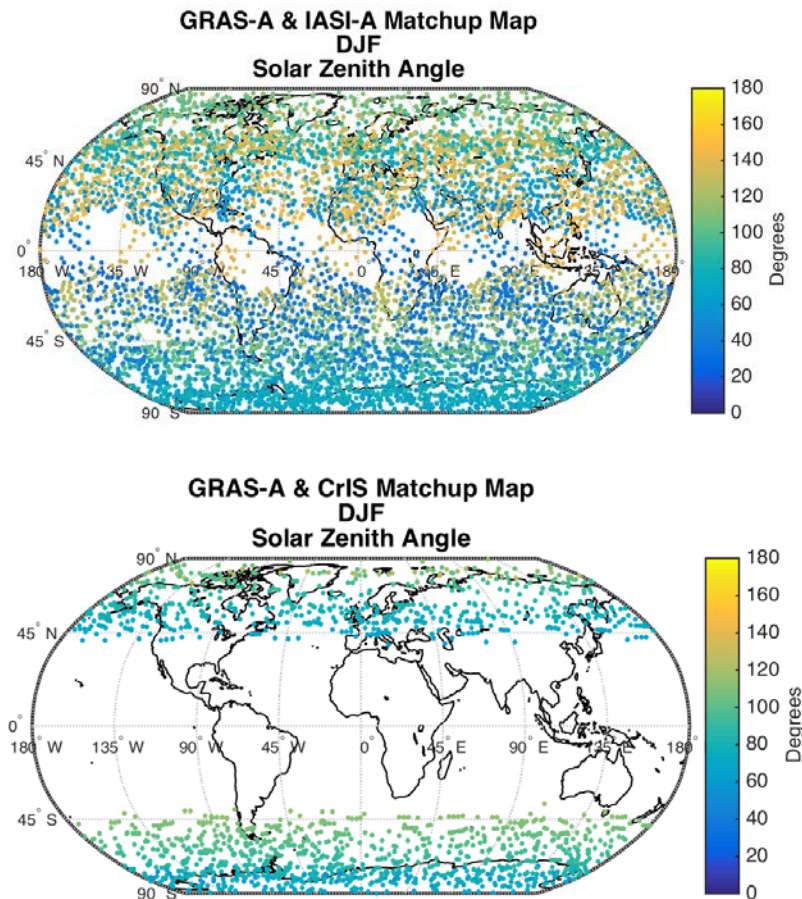


Figure 3.2. Maps of matchup locations colored by solar zenith angle for the DJF seasons of 2015 and 2016 for the GRAS-B and IASI-B comparison (top) and the GRAS-B and CrIS comparisons (bottom).

4. Radiative Transfer Calculations

Radiances and temperature Jacobians are calculated using the OSS RTM for each of the dry, wet, and background GRAS matchup temperature profile datasets. Parameters describing the atmospheric state, aside from air temperature, are held constant between the three RTM calculations for each matchup case. Focus is confined to the 15 micron carbon dioxide absorption region—Table 4.1 and 4.2 list the channels for which calculations are performed in addition to characteristics of their weighting functions (WFs).

As the RTM does calculations over fixed pressure levels, a pressure profile is calculated for the RO dry temperature using the following equation:

$$p_{\text{dry}}(z_g) = T_{\text{dry}}(z_g) * N(z_g) / 77.6 \quad (1)$$

where z_g is geopotential height coordinate, N the refractivity, and T_{dry} the dry temperature [Danzon *et al.*, 2014]. The dry, wet, and background RO temperatures are then interpolated to the defined RTM pressure grid, but they do not cover the entire vertical domain of the model, which extends from 1100 – 0.005 hPa, so a climatology is needed to fill in missing data locations. For this purpose, the five Air Force Geophysics Laboratory (AFGL) model atmospheres are used [Anderson *et al.*, 1986]. To ensure that the RTM input temperature profiles are ‘smooth’, i.e. the RO and AFGL data are combined in a continuous way, the lapse rate of the AFGL profile is used to extrapolate the RO temperatures. Figure 4.1 shows seasonally, zonally averaged input temperature profile statistics. Even though the GRAS dry temperature standard deviation increases at altitudes above 30 hPa to be larger than the wet and background temperature standard deviations, the average of the merged RO interpolated dry and AFGL climatology profiles is structurally similar to the merged wet and background profiles, with maximum differences of ~10 K at or above 1 hPa.

This extrapolation method is also used for other RTM input profiles – specifically those defined using the ERA Interim reanalysis, which is used to define skin temperature, surface pressure, and ozone and water vapor profiles. The reanalysis values are bilinear interpolated to the location of the RO profiles and then linearly interpolated in time. Carbon dioxide profiles are defined using monthly, 2 degree zonal values from the CarbonTracker model, and then extended to be constant with height to fill in the pressure levels with missing values. Surface emissivity is defined by a fixed, constant ocean emissivity spectrum, and a perturbation study in the Appendix (Section 8) shows that the IR channels used in this study are not sensitive to this parameter. A default solar zenith angle of 89° is used, and radiances are simulated for the view angle corresponding to the mean scan angle of the matchup observed radiance measurement footprint. A perturbation study on the sensitivity of the studied channels to the temperature of pressure levels where RO data is typically missing is contained in Section 5.3 and provides an assessment of the uncertainty introduced to the radiance calculation from the use of a climatology.

Uncertainties due to missing data exist in general for channels whose weighting functions (WFs) peak at altitudes higher than the ~10 hPa (~30 km) level. Largest sensitivities to missing data treatment are seen in channels whose WFs peak in the upper stratosphere, while channels with lower peaking WFs are sensitive by an amount which is negligible for this study.

Table 4.1. Channel definitions for CrIS and IASI instruments used in this study. For the annually, globally averaged dry temperature Jacobians, the weight below 1 hPa and pressure of level of the maximum is shown.

CrIS									
Channel #	8	18	21	26	28	29	30	31	32
Wavelength (microns)	15.282	15.137	15.094	15.024	14.995	14.981	14.967	14.953	14.939
Wavenumber (cm-1)	654.38	660.63	662.50	665.63	666.88	667.50	668.13	668.75	669.38
Weight Below 1.2 (0.34) hPa	1.00 (1.00)	0.99 (1.00)	0.89 (0.96)	0.97 (0.99)	0.99 (0.99)	0.64 (0.90)	0.66 (0.91)	0.87 (0.98)	0.90 (0.98)
WF Max (hPa)	66.1	56.1	12.6	35.7	26.2	1.3	1.7	4.9	11.0

33	35	36	51	52	57	70	75	77
14.925	14.898	14.884	14.679	14.665	14.599	14.427	14.363	14.337
670.00	671.25	671.88	681.25	681.88	685.00	693.13	696.25	697.50
0.94 (0.99)	0.94 (0.99)	0.97 (0.99)	0.98 (0.99)	0.98 (1.00)	0.99 (1.00)	0.99 (1.00)	1.00 (1.00)	0.99 (1.00)
7.0	14.5	51.5	35.7	56.1	66.1	110.2	160.5	180.0

Table 4.2. Same as Table 4.2 except for IASI.

IASI										
Channel #	88	89	90	91	92	93	94	95	96	97
Wavelength (microns)	14.998	14.993	14.987	14.981	14.976	14.970	14.965	14.959	14.953	14.948
Wavenumber (cm-1)	666.75	667.00	667.25	667.50	667.75	668.00	668.25	668.50	668.75	669.00
Weight Below 1.2 (0.34) hPa	0.98 (0.99)	0.96 (0.99)	0.81 (0.95)	0.62 (0.91)	0.59 (0.89)	0.64 (0.91)	0.71 (0.93)	0.78 (0.96)	0.84 (0.97)	0.88 (0.98)
WF Max (hPa)	32.3	23.5	1.7	1.7	1.7	1.7	2.2	2.7	3.3	8.2

98	99	100	105	106	108	109	199	205
14.942	14.937	14.931	14.903	14.898	14.887	14.881	14.399	14.368
669.25	669.50	669.75	671.00	671.25	671.75	672.00	694.50	696.00
0.91 (0.98)	0.92 (0.98)	0.91 (0.98)	0.96 (0.99)	0.94 (0.99)	0.97 (0.99)	0.98 (1.00)	0.99 (1.00)	0.99 (1.00)
9.5	9.5	8.2	26.2	16.4	35.7	61.0	160.5	190.3

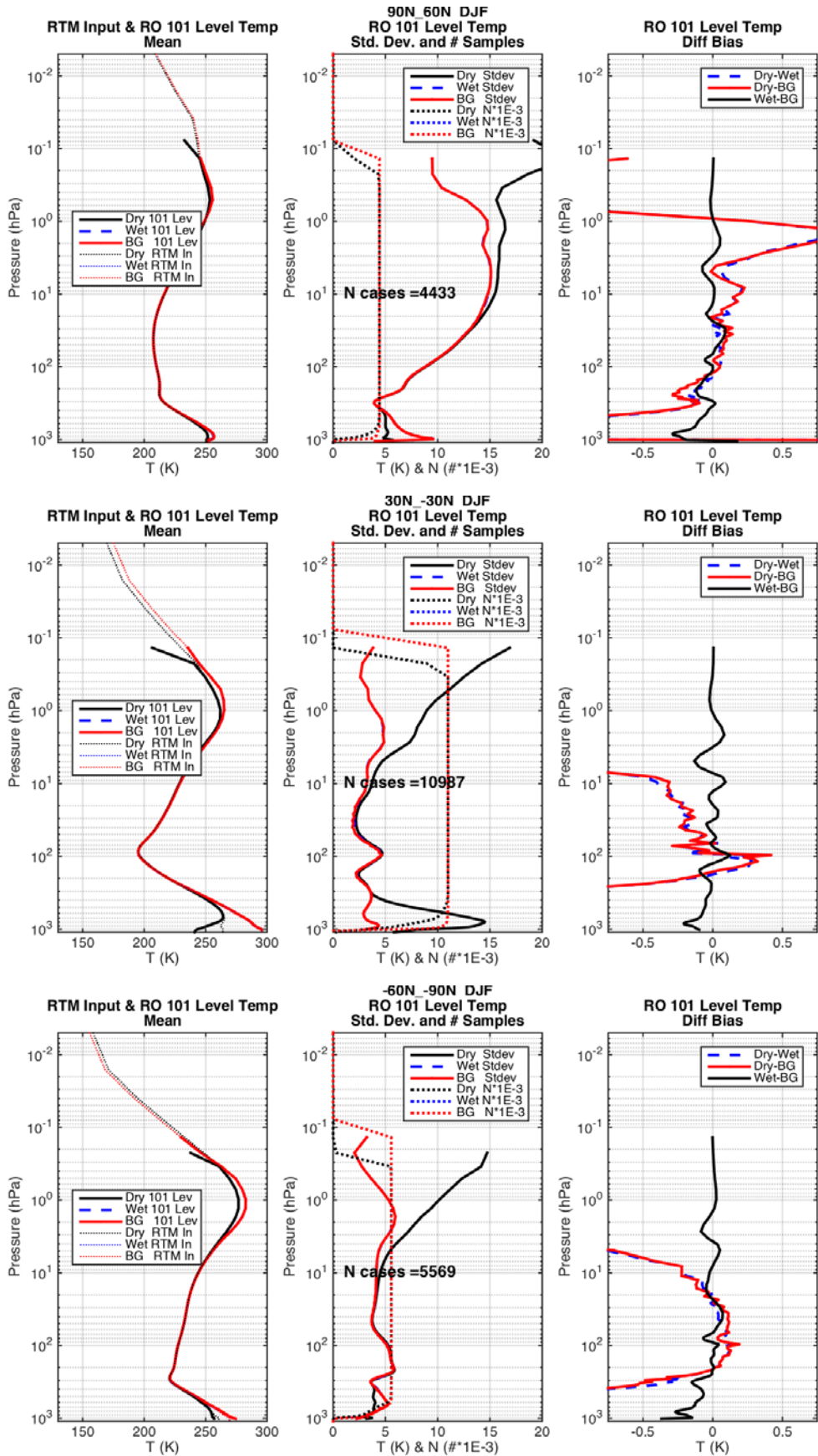


Figure 4.1. Seasonally, zonally averaged GRAS–A temperatures for the IASI-A matchup dataset for the DJF Arctic (top row), Tropics (middle row), and Antarctic (bottom row) zones. Left panels show dry (black), wet (blue), and background (red) temperatures interpolated to 101 pressure levels (bold) and with the climatology extrapolation added (thin, dotted). Middle panels show the 101 level dry, wet, and background temperature standard deviations (solid, dashed) and number of samples scaled by $1E-3$ (dotted). Right panels show difference biases of dry minus wet (blue, dashed), dry minus background (red), and wet minus background (black).

5. Uncertainty Analysis

Quantitative uncertainty estimates, representing stochastic errors, are defined in BT space for different elements of the comparison including the CrIS and IASI observations, RO temperature profile products, and various components of the RTM calculations. These components are then combined into a total BT uncertainty estimate, u_{total} , by using the following equation and assuming they are independent and have normal distributions:

$$u_{\text{total}} = \sqrt{[u_{\text{RTM_model}}^2 + u_{\text{IR_obs}}^2 + u_{\text{RO_extrap}}^2 + u_{\text{RO_temp}}^2]}. \quad (2)$$

This uncertainty represents a stochastic error estimate, not a systematic error. If the difference between the IR observed BTs and RO calculated BTs is less than the u_{total} value, then it is said the RO temperature products are in agreement with the IR observations. It is stressed that this definition of agreement does not take systematic errors into account, but it represents the single sample, random error, and is therefore compared to the standard deviation of the calculated minus observed BTs. The u_{total} estimate is computed separately for the dry, wet, and background temperatures for 5 zonal atmospheres and the four meteorological seasons. The following sections describe how each error component is defined.

5.1 RTM Model Errors

The uncertainty produced in the RTM calculation process is estimated by a constant with wavenumber value that is similar for each of the dry, wet, and background temperatures. The OSS model is tuned to agree with the reference Line-by-Line RTM to within 0.05 K [Moncet *et al.*, 2015], and it is then assumed that a 0.05 K uncertainty is associated with the Line-by-Line RTM calculations to obtain a 0.1 K value for the $u_{\text{RTM_model}}$ uncertainty component for all zones, seasons, and channels. This value is also used to include uncertainty associated with definition of the carbon dioxide profile and its impact on the calculations.

5.2 IR Observations

Values of the IR sounder instrument noise for both CrIS and IASI are estimated to be ~0.5 K for spectral channels used in this study at the longwave edge of the 15 micron CO₂ band [Zavyalov *et al.*, 2013]. This value represents an expected stochastic error for the IR radiance measurements and is used to define the $u_{\text{IR_obs}}$ term. This value is distinct from systematic errors which have been found for both CrIS and IASI to be under 0.5 K by numerous studies [Tobin *et al.*, 2013; Wang *et al.*, 2015; Aumann *et al.*, 2008; Blumstein *et al.*, 2007; Goldberg *et al.*, 2009; Illingworth *et al.*, 2009; Larar *et al.*, 2010; Newman *et al.*, 2012; Wang *et al.*, 2010; Wang *et al.*, 2015].

5.3 RO Extrapolation Errors

This $u_{\text{RO_extrap}}$ component represents the potential error that could come from the temperature climatology used to extend the RO profiles to higher levels of the atmosphere prior to RTM calculations. To calculate this amount the degree to which the BT calculations are sensitive to the temperature of specific vertical regions of the atmosphere

needs to be quantified using the IASI and CrIS temperature Jacobians. For each IR channel, the percent of weight of the Jacobian from altitudes for which the AFGL climatology lapse rates define the RTM input profiles is calculated. These values are then used to weight the five AFGL model atmosphere's BT spectra. The resulting 'residual spectra' represent the total radiance contribution from the subset of TOA temperature levels. Because the hypothetical radiance contribution from a 'truth' temperature at these levels does not represent an error, the weighted radiances are multiplied by a factor 0.08, representing an 8% error in the climatology (translating to ~12-20 K), to obtain the u_{RO_extrap} uncertainty components. The percent error magnitude is defined by the approximate maximum difference between the seasonally, zonally averaged RTM input dry and wet/background profiles at altitudes where climatology is used (example can be seen in middle row panel of Fig 4.1 at altitudes above ~0.3 hPa).

The pressure levels which mark the RO wet/background and dry profile top of atmosphere values are typically 0.12 hPa and 0.34 hPa, or less respectively (i.e. or higher in altitude). The Jacobian's weights used for the dry, wet, and background u_{RO_extrap} calculations are for altitudes above the 0.34 hPa so that the weights represent a 'worst case scenario' situation (the contribution is defined to be larger than the truth, yielding a larger uncertainty). Table 4.1 and 4.2 show the weights of the CrIS and IASI annually and zonally averaged temperature Jacobians *below* the 0.34 hPa level respectively. The values used to weight the AFGL radiance spectra are equal to 1.00 minus these values. Numerous channels are found to have 1% or less weight coming from above the 0.34 hPa level, and it is channels such as these which are focused on in later analyses. Figure 5.1 shows the DJF temperature Jacobians for both CrIS and IASI for the Arctic zone.

Figure 5.2 shows the u_{RO_extrap} terms for both IASI and CrIS for the five AFGL atmospheres. For the channels of focus which have less weighting and contribution from the TOA levels (1% weighting or less), the uncertainty is estimated to be under 0.1 K. The polar summer and polar winter atmospheres have the largest and smallest uncertainties respectively—the warmer the stratopause, the larger the uncertainty.

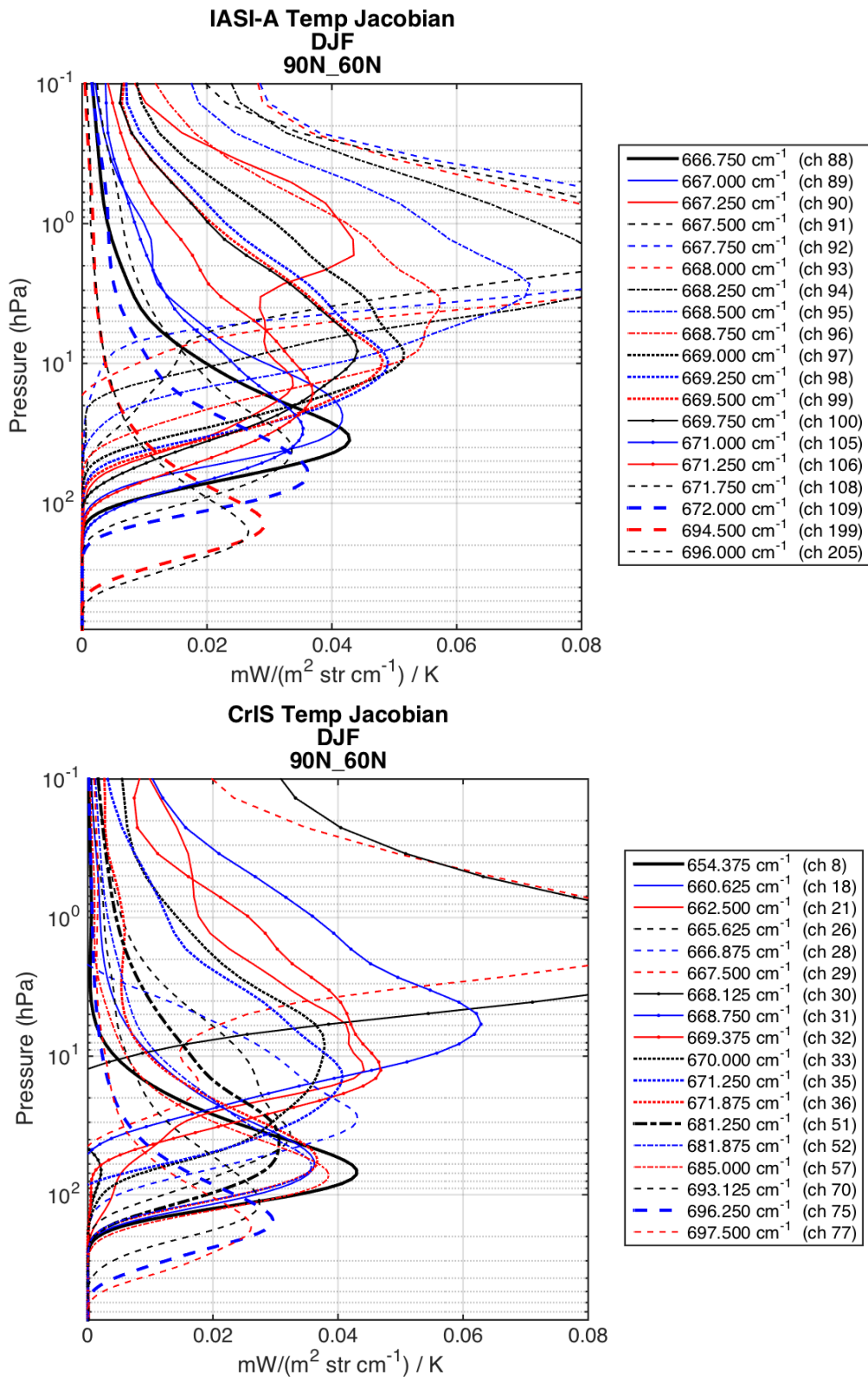


Figure 5.1 IASI (top) and CrIS (bottom) Artic, DJF averaged temperature Jacobians for the GRAS-A matchup datasets. Channels with bolded Jacobians with maxima between 200 and 30 hPa are focused on in later analyses.

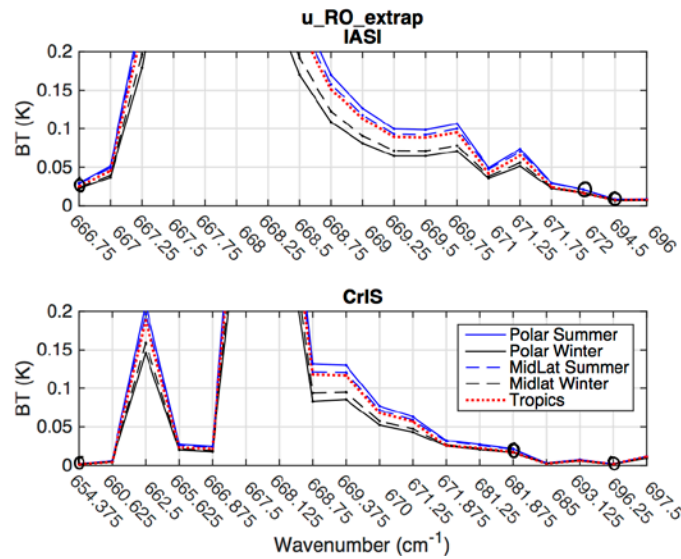


Figure 5.2 The u_{RO_extrap} term for IASI (top) and CrIS (bottom) for five AFGL atmospheres. Black circles highlight channels of focus.

5.4 RO Temperature

Stochastic temperature error estimates for the GRAS products are provided by the ROM SAF and are accounted for in the uncertainty analysis with the u_{RO_temp} component.

For the background and wet temperature profiles, error covariance matrices are used. A single, globally and annually representative error covariance defines the background profile errors, and though error estimates are provided for each individual wet temperature profile, this study uses representative covariance matrices for five latitude zones and four seasons. Wet error covariances are computed using data from single days—January, April, July, and October 15th—and are seen to be robust when the datasets are split in half. These error matrices are used in combination with seasonally, zonally averaged temperature Jacobians to compute associated BT errors using the following equations:

$$\mathbf{U}_{RO_temp} = \mathbf{K}\mathbf{B}\mathbf{K}' \quad (3)$$

$$u_{RO_temp} = \text{sqrt}(\text{diag}(\mathbf{U}_{RO_temp})) \quad (4)$$

where \mathbf{K} is the normalized temperature Jacobian, \mathbf{B} is the RO temperature error covariance, \mathbf{U}_{RO_temp} is the RO BT error covariance, and ' is the transpose.

Since the RO wet and background temperature products are provided on dynamic model levels which span from the surface to ~ 0.1 hPa and the calculated temperature Jacobians are defined on the fixed RTM pressure grid which spans from 1100 – 0.005 hPa, either the \mathbf{K} or \mathbf{B} matrix needs to be re-defined on the other's pressure grid. As the \mathbf{K} matrix has only one dimension in pressure, its chosen to interpolate the Jacobians into the RO error pressure domain. Representative pressure profiles for the error covariance matrices are computed from monthly averages of pressure profiles corresponding to the matchup datasets, and the temperature Jacobians are then interpolated using these and multiplied by a correction factor matrix for the interpolation from one grid to another. Due to the

similarity in the temperature Jacobians from the Metop-A and Metop-B matchup datasets, the two datasets for each IASI and CrIS are averaged together to obtain two representative Jacobian sets – one for IASI and one for CrIS.

The background and wet temperature error covariance matrices are shown in figure 5.3 for the December, January, and February (DJF) Arctic zone. The background covariance matrix diagonal has maxima near the surface and top of atmosphere, with a general minimum in the UTLS region of interest. Similar features exist in the wet error covariance. For both the background and wet temperatures, nearby levels are anti-correlated at altitudes higher than 4 hPa in the upper atmosphere, and very minimally correlated from ~4 - 700 hPa.

Figure 5.4 shows the background and wet temperature errors (the square root of the covariance diagonal) as profiles for the DJF and JJA seasons. The wet error profiles are all decreased in comparison to the background within the 10 – 100 hPa region. The background error is between 0.25 and 1 K in the 20- 600 hPa range. All wet error profiles are ~0.3 +/- 0.05 K from 30–100 hPa. The error for each zone and season starts to increase with decreasing altitude under the tropopause level, with the tropical error reaching the highest values of ~0.6 K above the 300 hPa level. Figure 5.5 shows the resulting RO background and wet BT errors for both CrIS and IASI. Though the background and wet results look very similar, the background are at least ~0.01 K larger across all wavelengths. Both the IASI and CrIS uncertainties reach a maximum of ~0.40-0.45 K for the channels whose Jacobians have contribution from higher altitudes of the atmosphere. For channels of focus in this study, however, the wet and background errors for all atmospheres are confined under 0.20 and 0.25 K respectively.

For the GRAS temperature dry product, though no error covariance matrices or profile-by-profile error estimates are provided, a general quality requirement in the form of a percent accuracy profile is defined. This percent error is used to perform a sensitivity study on the BT calculations to calculate corresponding dry temperature BT errors. For 5 control atmospheres, two perturbations to the temperature are performed by adding or subtracting the stochastic dry error estimates which are shown in Figure 5.6. Control profiles are defined by the AFGL atmospheres (used to extrapolate RO temperatures). The dry temperature error percent is estimated as 2% at sea-level falling linearly with altitude to 0.2 % at the tropopause, and above the tropopause it is 0.2%. The right panel of Fig 5.6 shows the control and perturbation temperature profiles. Dry error estimates have a maximum of ~6 K at the surface, but in the 30-300 hPa range are decreased to ~0.45 K for all profiles with the exception of the tropics, which is ~2 K at 300 hPa.

Fig 5.7 shows the corresponding control minus perturbation BT spectra. Differences for the added and subtracted dry errors are symmetrical about 0 K. The magnitude of the differences is generally 0.5 K. Exceptions to this exist for wavenumbers greater than 685 cm^{-1} which have contribution from lower parts of the atmosphere. Here the differences reach their maximum value of ~1K in the tropical atmosphere. Lastly, to define the dry $u_{\text{RO_temp}}$ term, the two perturbation sets (the dry error addition and subtraction) are averaged together after the absolute value is taken, and the appropriate AFGL atmospheres are assigned to the seasonal, zonal uncertainty dimensions.

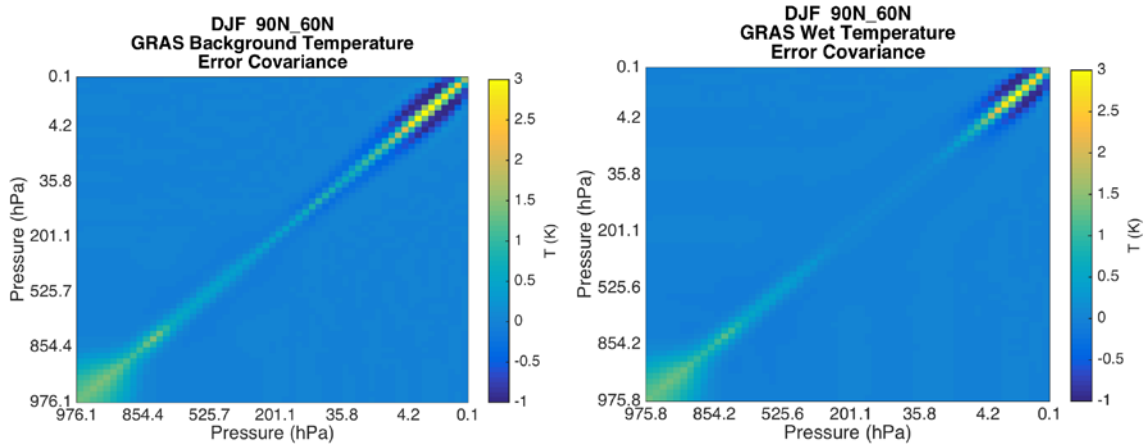


Figure 5.3 GRAS global, annual background temperature error covariance matrix plotted on pressures corresponding to the DJF Arctic (left), and the GRAS DJF Arctic representative wet temperature error covariance (right) in temperature space.

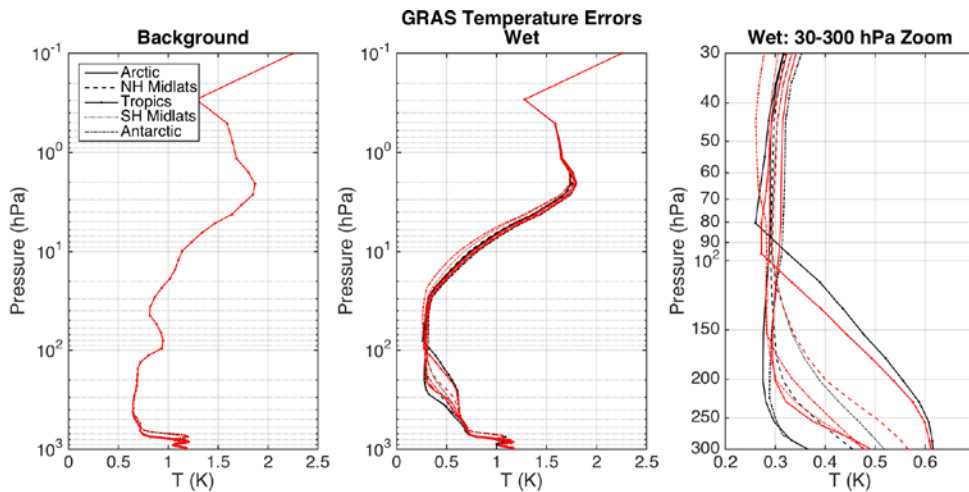


Figure 5.4 GRAS background (left), and wet (middle, and right zoomed) stochastic temperature error profiles for each of the 5 zones overlaid for the DJF (black) and JJA (red) seasons.

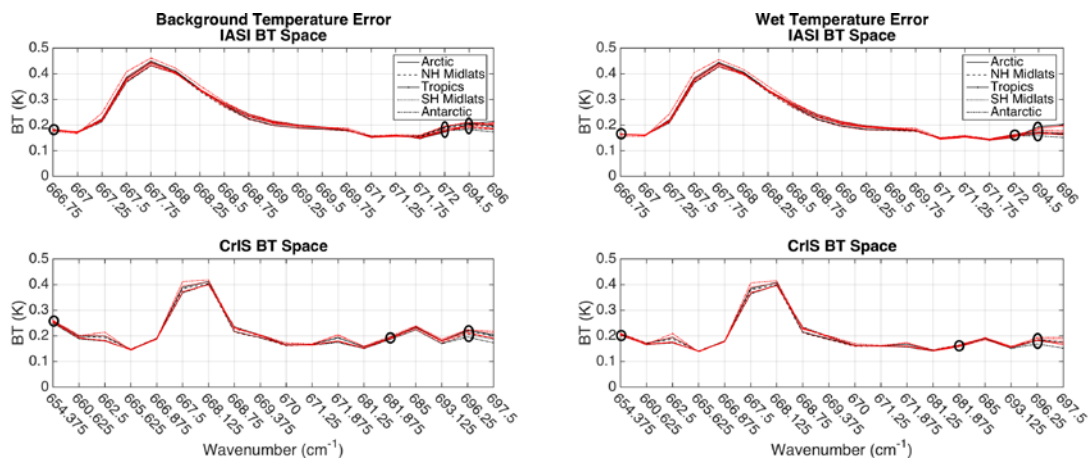


Figure 5.5 GRAS background (left) and wet (right) stochastic temperature errors converted into BT space for IASI (top) and CrIS (bottom) for five zones for the DJF (black) and JJA (red) seasons.

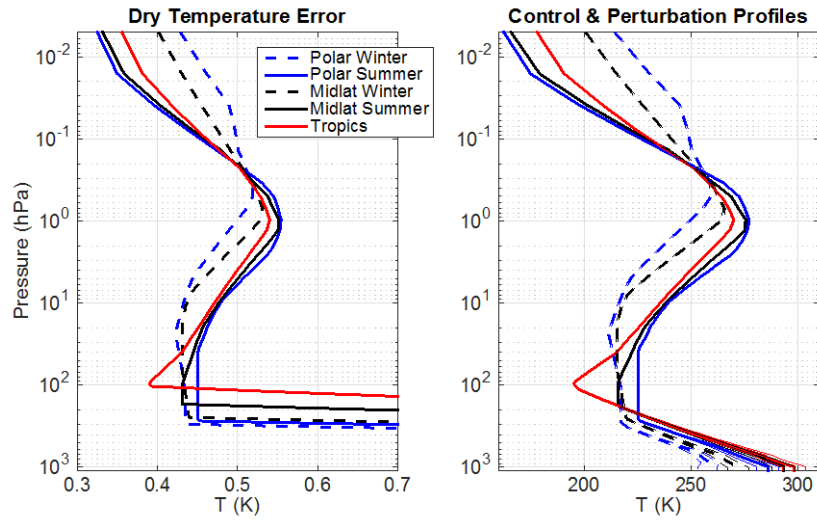


Figure 5.6 GRAS dry temperature stochastic error estimates (left) and control (thick) and perturbation (thin) temperature profiles (right, overlaid) used to compute corresponding BT errors for five AFGL atmospheres.

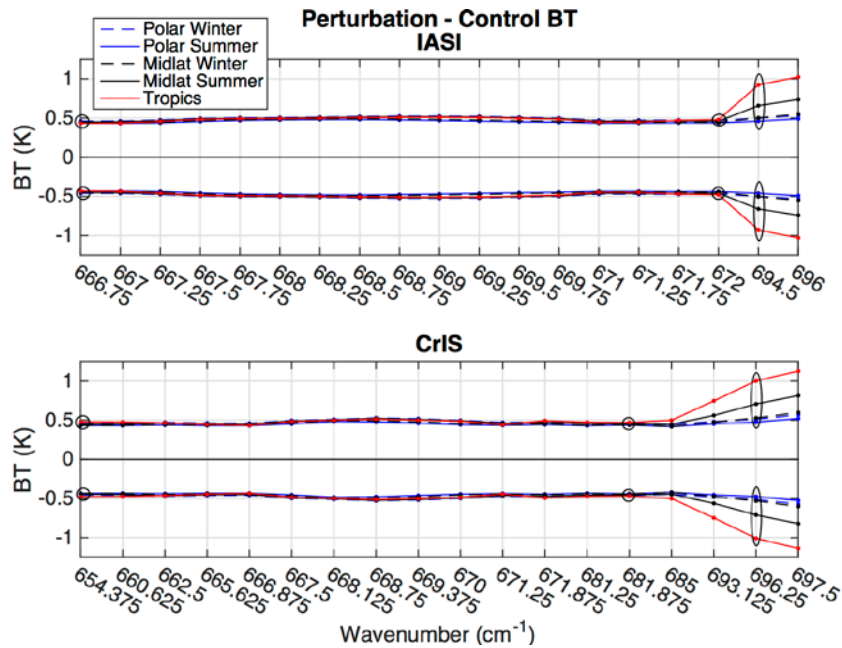


Figure 5.7 GRAS dry temperature stochastic error in BT units for IASI (top) and CrIS (bottom) for five AFGL atmospheres.

5.5 Total Uncertainty

After combining the four uncertainty components which represent stochastic errors, there is a total BT calculation uncertainty estimate for each the dry, wet, and background temperatures for all seasons and zones. Results for DJF and JJA seasons are shown for IASI and CrIS analyses in Fig 5.8 and 5.9 respectively. Background and wet uncertainties for both IASI and CrIS look very similar, with total uncertainties being ~ 0.55 K for channels of interest. The dry uncertainties for all channels are larger than the wet and background estimates, being between ~ 0.65 and 0.7 K for most channels, and they show increased uncertainties for wavenumbers above 685cm^{-1} , with the tropics reaching the maxima of up to 1.2 K.

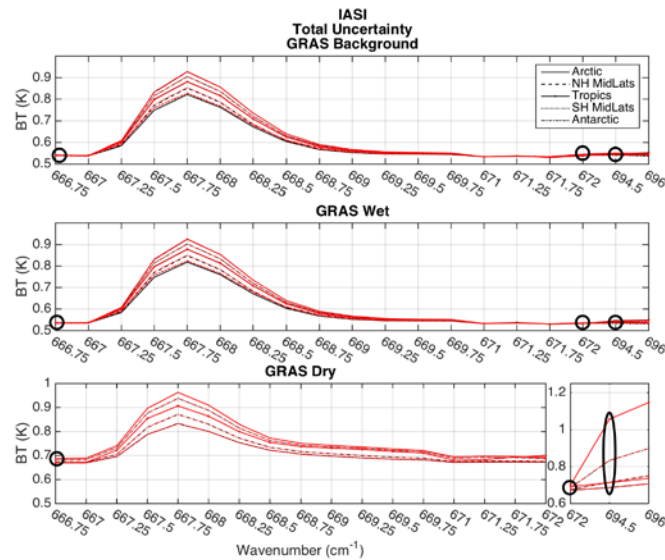


Figure 5.8 Total BT uncertainty component, u_{total} , for the IASI match-up analysis for the GRAS background (top), wet (middle), and dry (bottom) temperatures for DJF (black) and JJA (red) seasons. This uncertainty represents a stochastic error. Note y-scale changes between panels and wavenumber breaks.

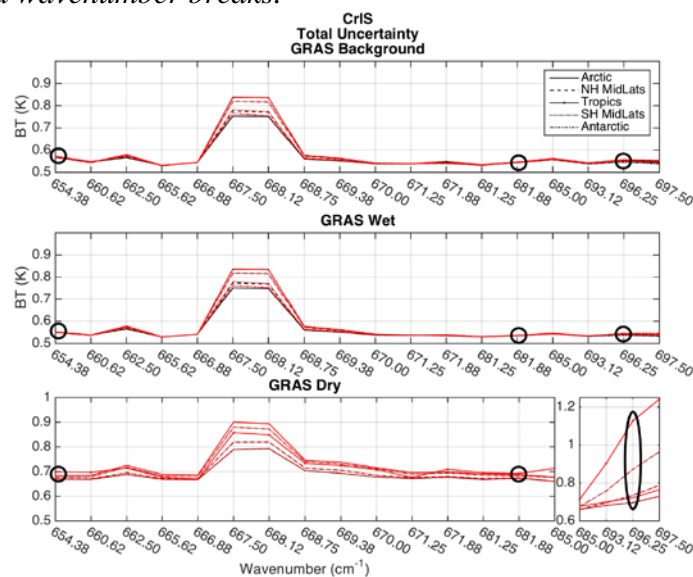


Figure 5.9 Same as above, except for CrIS analysis. Note y-scale changes between panels and wavenumber breaks.

6. IR and RO BT Comparisons

6.1 Methods

For the BT comparison, differences are taken as RO calculated minus IR observed. The four matchup datasets have differences for each the dry, wet and background temperatures. The bias, standard deviation, and uncertainty of the bias are found for all sets of differences over 2015 through 2016 on various temporal scales for 5 latitude zones. Latitude zones span 30 degrees, except for the tropical zone which spans 60.

6.2 Results

6.2.1 Seasonal

Figure 6.1 shows the GRAS calculated minus IR observed BT statistics for the dry temperature product for all zones, seasons, and matchup datasets for two representative pressure levels—the ~150 hPa level (IASI channel 199/694.5 cm^{-1} , CrIS channel 75/696.25 cm^{-1}) in the lower stratosphere and the ~30 hPa level (IASI channel 88/666.75 cm^{-1} , CrIS channel 51/681.25 cm^{-1}) in the upper-middle stratosphere. Standard deviations of calculated minus observed BTs are shown overlaid with the total BT uncertainty estimate, which is based off of stochastic errors, in the left panels with biases in the right panels. Results are shown for channels whose weighting functions have ~1 % weight from altitudes above 0.34 hPa. For both IASI and CrIS sensors, the Metop-A and Metop-B GRAS matchup biases are within ~0.1 K, and standard deviations are within 0.25 K (often within 0.1 K)—revealing a consistency between the Metop datasets, with the CrIS datasets being more similar overall. A constant, ~0.1 K, offset between the IASI-A and IASI-B BT biases across all zones and seasons is seen. Previous work [Jougllet *et. al*, 2014] shows that IASI-A and IASI-B are indeed biased with respect to each other by such a constant amount and has also shown that IASI-A is less biased with respect to AIRS and CrIS. To capture the broader variation of the IR observations, and due to the similarity of the Metop-A and – B datasets (with the exception for the IASI’s approximately constant with wavenumber offset), the following results focus on the IASI-B/GRAS-B and CrIS/GRAS-B datasets. Though the CrIS and IASI datasets are not expected to give similar results due to the different equator crossing times of their platforms and their different WF shapes, their dry biases are within ~0.5 K of each other, often within 0.25 K. However, at ~30 hPa, the CrIS matchup datasets have consistently smaller standard deviations than the IASI datasets, on average by ~0.25 K. Comparison of the difference standard deviations and BT uncertainties over height shows that at ~150 hPa, the standard deviation is consistently within 0.25 K of its expected value, being larger than expected by ~0.25 K in the JJA/SON Antarctic and by ~0.2 in the DJF/MAM tropics. At ~30 hPa, IASI standard deviations are larger than the uncertainties across all zones and seasons—the BT uncertainty estimate does not account for all of the stochastic error sources in the GRAS-IASI BT differences for that channel, though CrIS standard deviations have overall much closer values to the BT uncertainty estimates. Comparison of the ~150 and ~30 hPa level results also reveals the difference biases change with height—for example the tropical biases change from positive to negative with increasing height. The vertical dependence of the statistics is investigated more closely in the following figures using more channels.

Figures 6.2 and 6.3 show the GRAS-B minus IASI-B matchup BT biases and standard deviations for the DJF and JJA season respectively for all latitude zones. The calculated minus observed BT biases and standard deviations are plotted at the height of the channels WF maxima, and the panels are focused on the 10-300 hPa (~10-30 km) region. Error bars mark the calculated BT uncertainty and color indicates the RO product, i.e. dry, wet, or background GRAS temperature. Wet and background biases are very similar, and in general they are closer to zero than the dry biases, especially in polar summers at altitudes above 30 hPa. Their standard deviations are also similar, generally being constant with height and around 0.5 K. It is expected that the BT wet and background uncertainties would also hold this structure if the BT uncertainty estimate correctly accounted for the stochastic errors, and this is confirmed in general in the JJA/DJF mid-latitude zones and polar winter regions. Polar summer regions have standard deviations which are slightly less, by ~0.1 -0.2 K, than the BT uncertainty, while tropical regions have slightly larger standard deviations, by ~0.1 K, than the BT uncertainties. This indicates that in the polar summer region, single-sample random error is less than expected, and in the tropics the single-sample random error is larger than expected. In contrast, the calculated dry minus observed BT standard deviations tend to increase in height, ranging from ~0.5 K at 200 hPa to ~1.5 K at 30 hPa for all zones. This increase with height is not reflected in the dry BT uncertainties—a characteristic of the dry temperature error estimate which is defined to be constant with height above the tropopause, and the constant with wavenumber nature of the IR noise and RTM BT uncertainty. The BT uncertainty is, however, seen to be larger for IASI's two lowest altitude channels (below ~150 hPa) which have contribution from below the tropopause. These two channels show the best agreement between the BT uncertainties and standard deviations of all the channels. Channels with contributions from higher levels have a large disagreement between the dry minus observed standard deviations and uncertainty estimates, up to over 1.2 K in magnitude.

Comparison of the seasons in Figure 6.2 and 6.3 show qualitatively mirrored results across the equator—e.g. the DJF Antarctic and JJA Arctic results look similar. In the tropical zone, IASI channels with the lowest peaking WFs have biases that are very different from the channels with WFs peaks above 100 hPa. For these two out of family channels, the IR observations are colder than both the dry and wet/background calculated BTs, and the standard deviations are all greater than 1 K and larger than the BT uncertainties. This vertical region of the tropics presents complications for the IR radiative transfer calculations due to 1] the sharp temperature gradient of the tropopause that the channels' WFs span over, and 2] the increased water vapor below which tends to weight the observations to lower levels. The computed temperature Jacobians shown in Figure 6.4 for the tropical region illustrate aspects of this issue. Fig 6.4 shows that the temperature Jacobians for these channels in the tropics have two maxima, with a local minimum at the height of the tropical troposphere (see Fig 6.4 right panel for tropopause height). It also shows that the Jacobians have contribution from altitude levels as low as 500 hPa. This overall complication may extend somewhat into the mid-latitude zones where the atmosphere sometimes has characteristics of the tropical latitudes. At such low altitudes in the tropical region, it is also likely that water vapor has a non-negligible contribution to temperature—a previous study which compared RO and ECMWF fields shows that water vapor makes a 1 K contribution to temperature at ~11 km and 0.5 K at ~12 K in the tropics, which is approximately the region of the tropopause (about 100 hPa) [Danzer *et al.*, 2014].

Water vapor at these high altitudes could be a potential source of disagreement between the IR and RO BTs. Further investigation is required to interpret these channel's results.

Scatter plots in Figures 6.5 and 6.6 look at characteristics of the IASI-B/GRAS-B Antarctic and Tropical results more closely. Specifically, the IASI-B observed BTs are plotted against the calculated BTs for the DJF and JJA season at two pressures levels—the ~30 and 150 hPa levels. Correlations between the observations and calculations are listed in the subfigure legends, and calculated minus observed BT difference statistics are listed in the lower right corners. Antarctic results in Fig 6.5 show the polar summer ~30 hPa level dry product BTs are less correlated with the observations in comparison to the other levels. This is also seen in the more visibly spread data and in the higher standard deviation of the calculated minus observed BTs at this level, which is 1.3 K in comparison to the 0.7 K value at ~150 hPa. For both levels and seasons, the dry difference standard deviations are increased in comparison to the wet and background's—a characteristic which is also seen in Fig 6.6's tropical results. In Fig 6.6 results for the two seasons are more similar—the ~180 hPa level for both DJF and JJA have correlations of ~0.90 or less, difference standard deviations of 1.2 K, and scatters which are visibly biased. Again, these results from the low peaking WF channels are likely contaminated by poor radiative transfer calculations due to the challenging nature of the tropical UTLS region. The tropical upper levels have smaller wet and background difference standard deviations of 0.57 K and 0.65 K, and increased correlations of ~0.96 and 0.97. The dry product still has difference standard deviations of 1.2 K or larger and lower correlations than the lower levels of ~0.8.

Next, Figure 6.7 and 6.8 show the same plots as Fig 6.2 and 6.3 for the CrIS/GRAS-B BT dataset for the DJF and JJA season respectively. For both seasons the CrIS and IASI BT statistics—which are not expected to be exactly similar due to differences in the IR sounders equator crossing times - typically have very similar structure. For example, the DJF SH mid-latitude biases for both CrIS and IASI decrease with increasing height, being under 0.5 K at ~150 hPa and reaching ~-0.75 K at ~15 hPa. Likewise, the wet and background biases are very similar with the dry biases deviating from them, typically to be farther from zero, markedly in the DJF Antarctic zone. Additionally, characteristics of the standard deviations for both CrIS and IASI have resemblance, with the background and wet having similar values while the dry standard deviation increases with height for all zones. The implications of this increase with height to be larger than the estimated CrIS uncertainties is the same as was for the IASI results—the channels with contributions from higher altitudes (above the ~70 hPa level) have total dry BT uncertainty estimates that do not account for all random error sources.

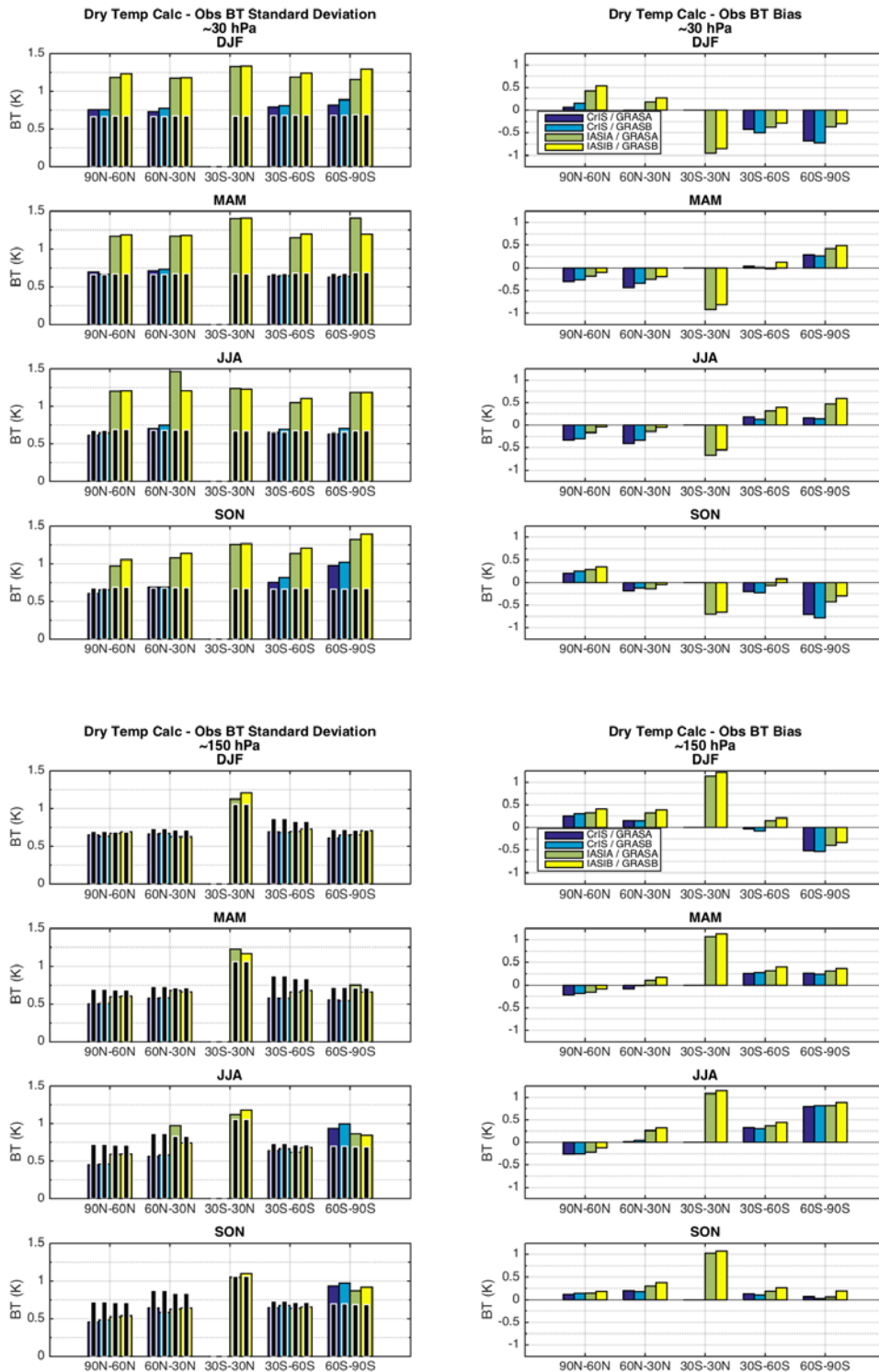


Figure 6.1 GRAS dry temperature computed minus observed BT biases (right column) and standard deviations overlaid by the total BT uncertainty estimate shown as black bars (left columns) for the ~150 hPa (bottom rows) and ~30 hPa (top rows) pressure level for the DJF season. Results for different matchup datasets are differentiated by color as listed in the legend.

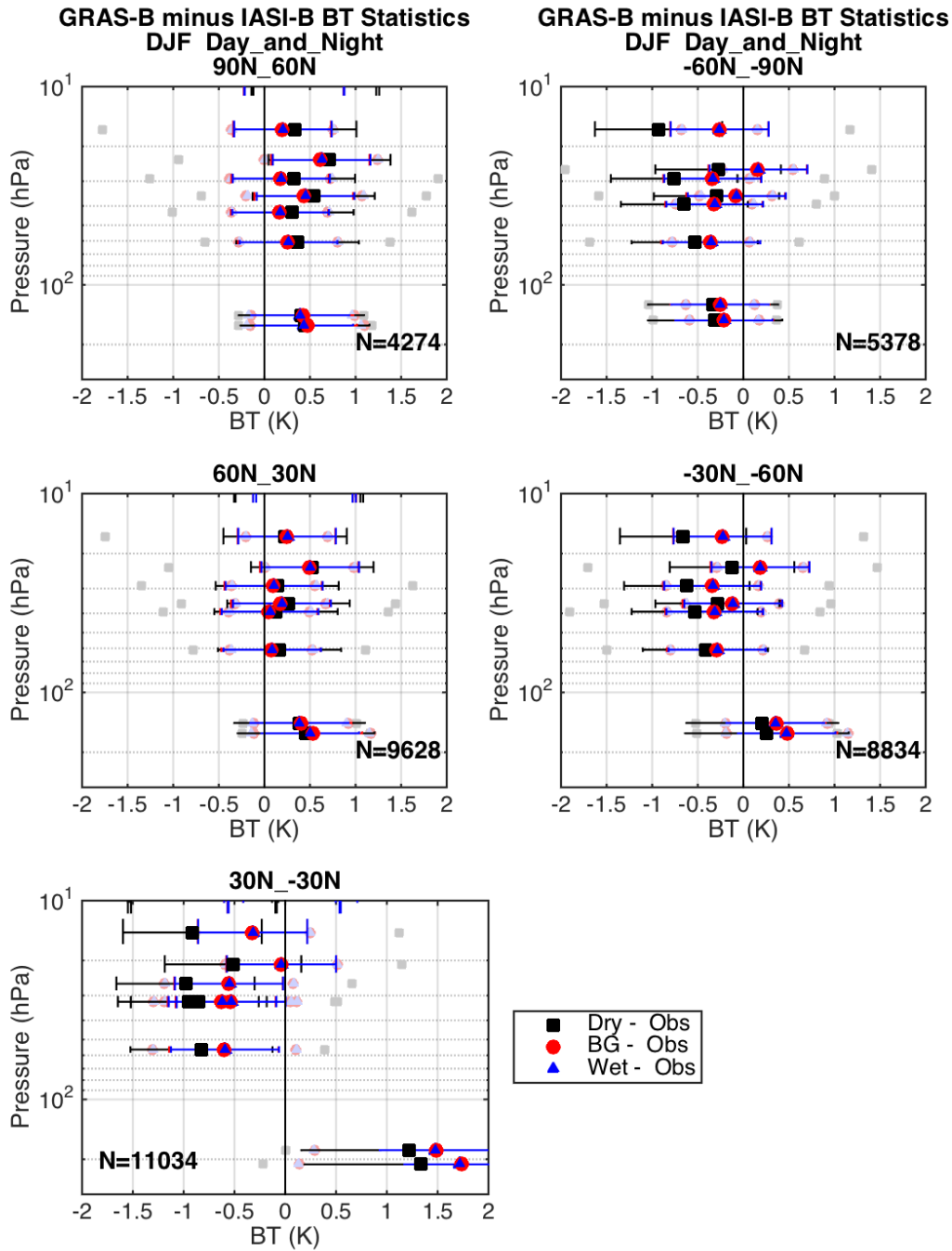


Figure 6.2 GRAS-B minus IASI-B BT biases (dark shade) and standard deviations (light shade, bounding the bias) for the DJF season and all latitude zones (split by panels) plotted at the height of the channels WF maxima. Dry (black square), wet (blue triangle), and background (red circle) biases are plotted with error bars marking the calculated BT uncertainties. Number of samples noted in figures as N.

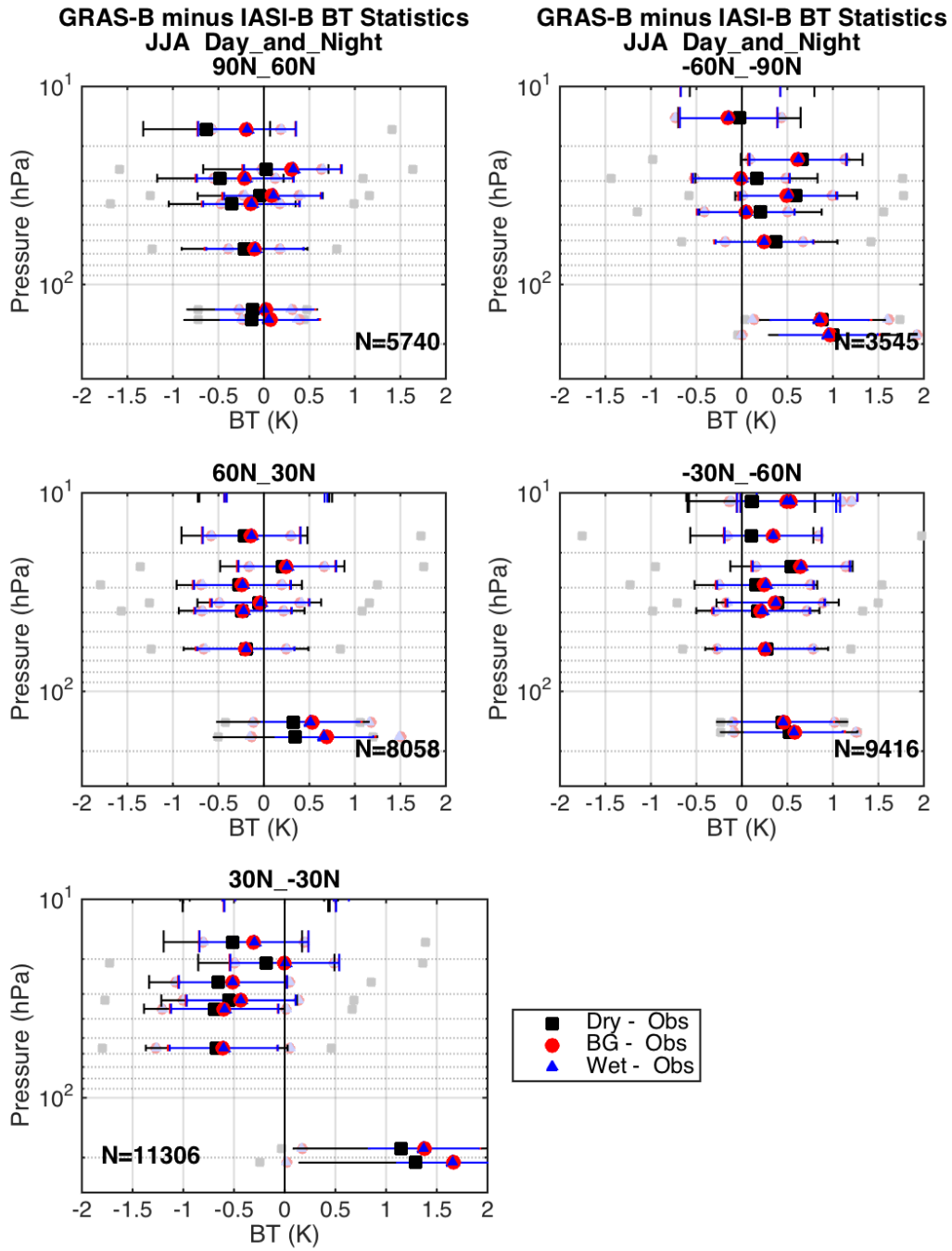


Figure 6.3 Same as Figure 6.2 except for the JJA season.

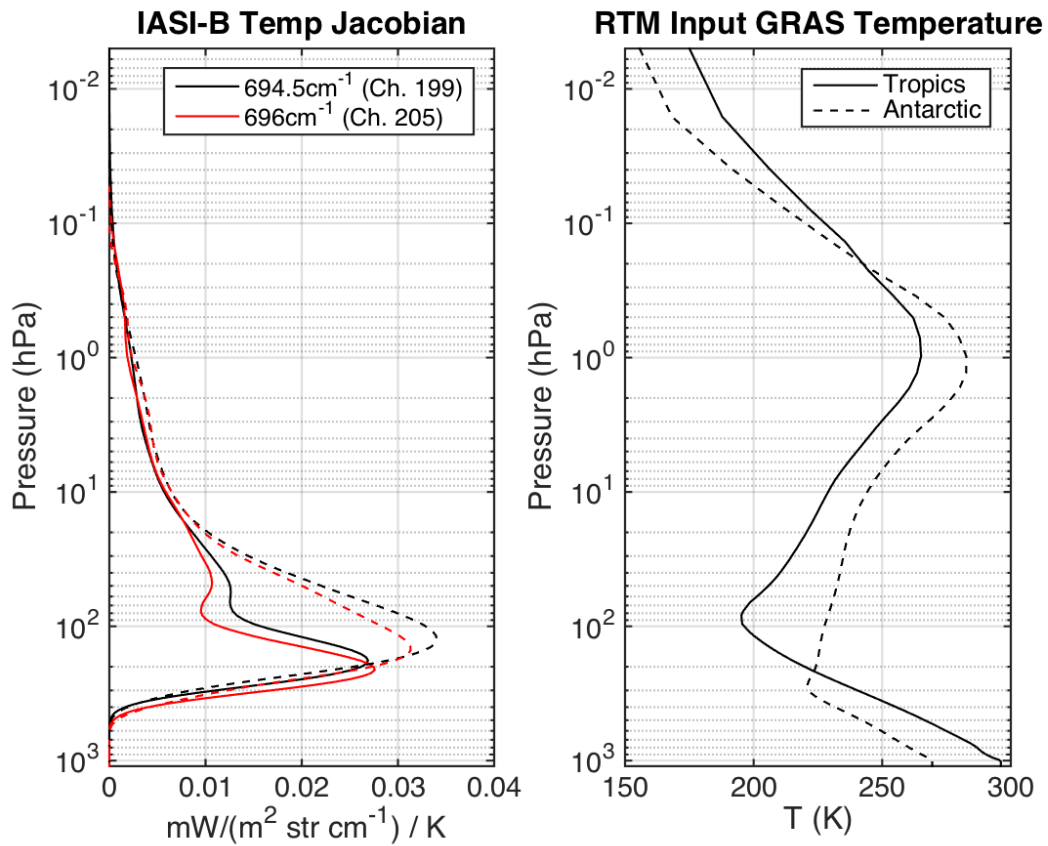


Figure 6.4 IASI-B/GRAS-B calculated background temperature Jacobians (left) and RTM input background temperatures (right) for the Tropics (solid lines) and Antarctic (dashed lines) for the DJF season. Figure illustrates the challenges of the radiative transfer techniques in the tropical UTLS region.

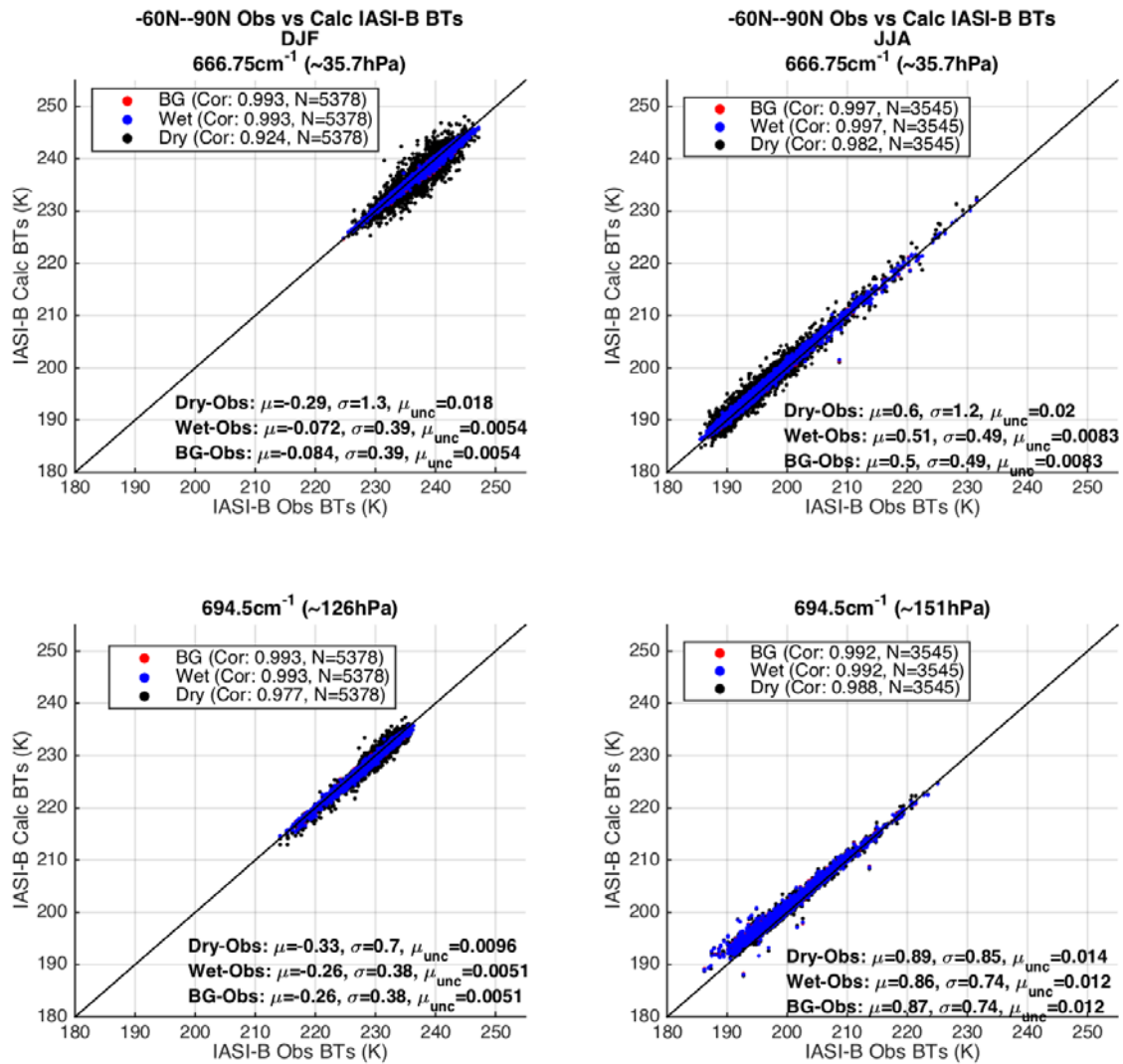


Figure 6.5 Antarctic IASI-B observed vs. calculated BTs for the DJF (left) and JJA (right) seasons for the ~30 hPa (top) and ~150 hPa (bottom) levels. Background (red), wet (blue) and dry (black) BT biases are overlaid. Correlations and number of samples, N, are listed in the legends. Calculated minus observed BT difference biases, standard deviations, and uncertainty of the biases are listed in the lower right corner of each panel.

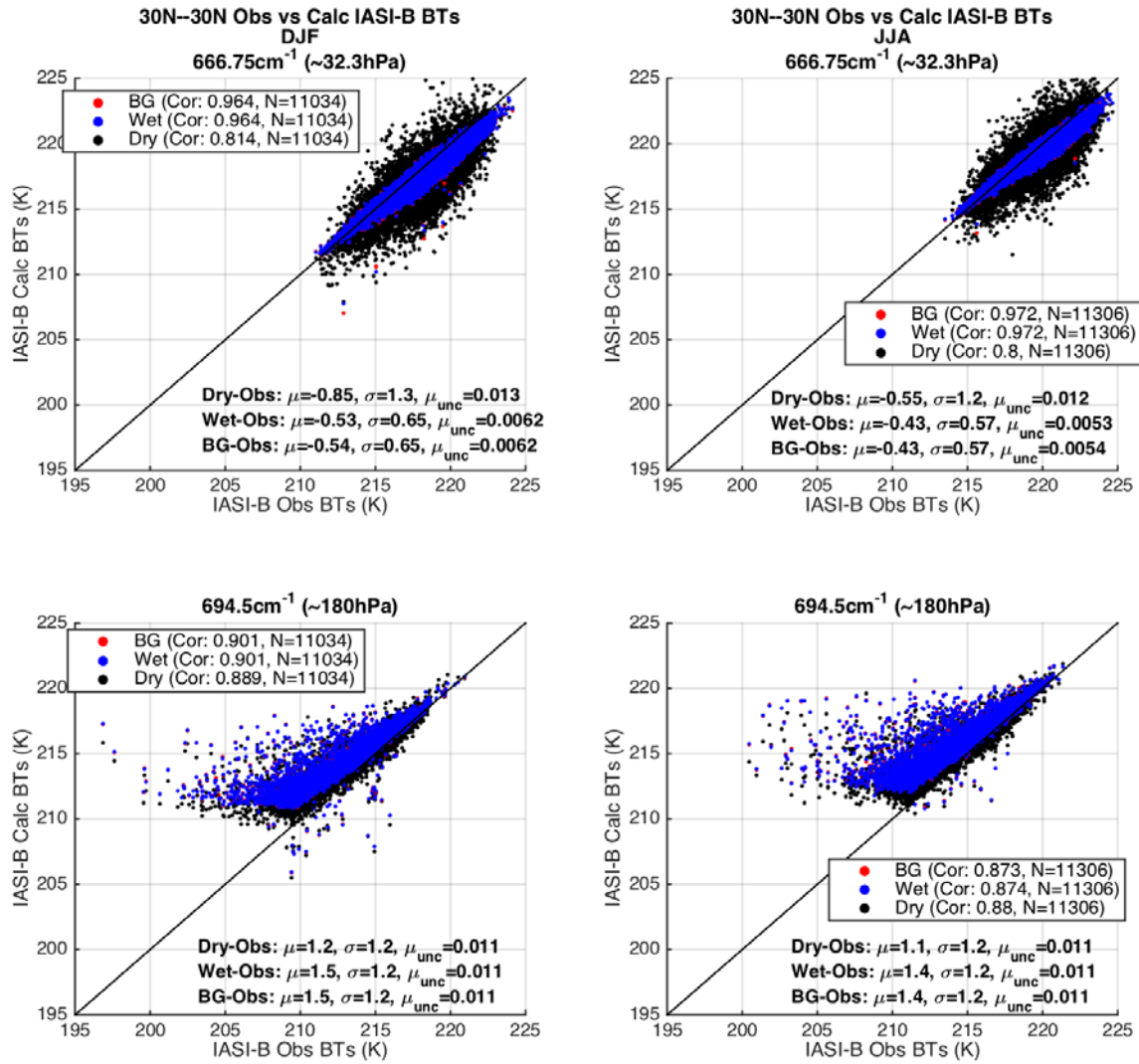


Figure 6.6 Same as Figure 6.5 except for Tropical zone.

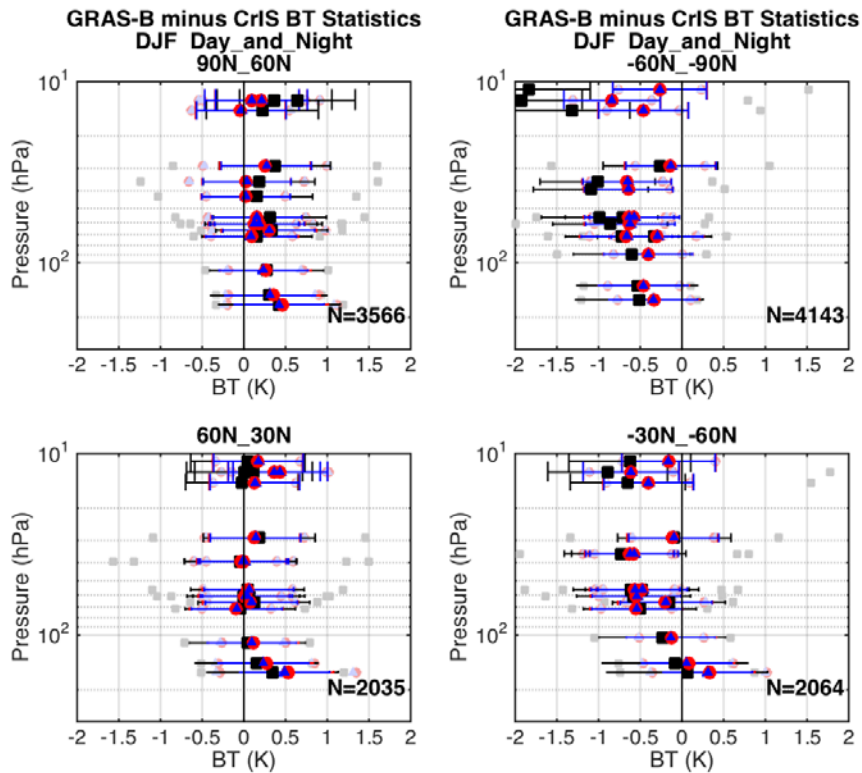


Figure 6.7 Same as Figure 6.2 except for the CrIS/GRAS-B matchup dataset. Tropical zone not shown due to insufficient sampling.

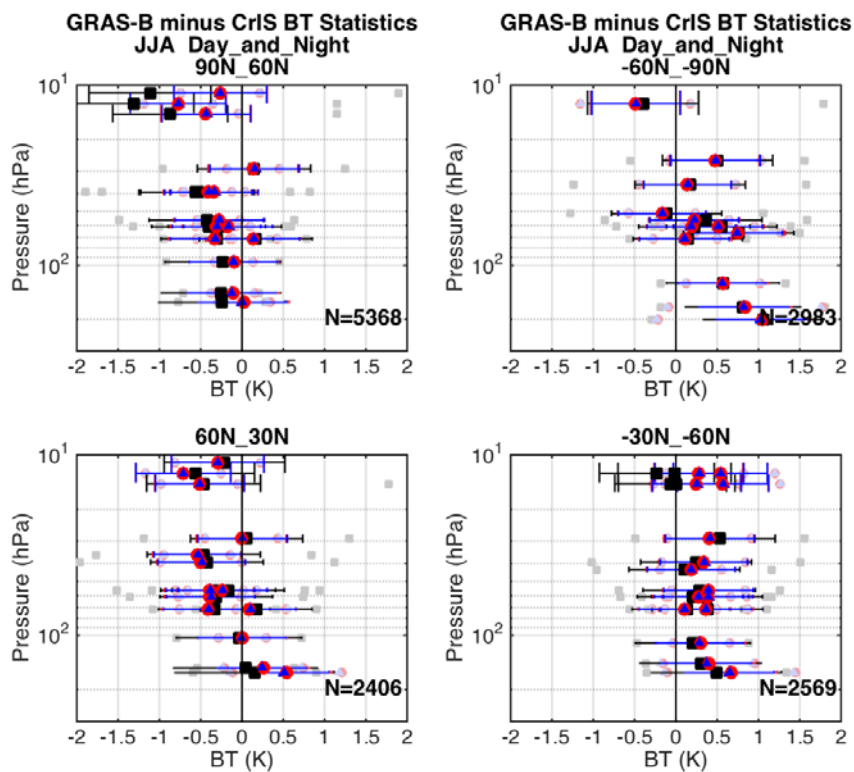


Figure 6.8 Same as Figure 6.2 except for the CrIS/GRAS-B matchup dataset and JJA season. Tropical zone not shown due to insufficient sampling.

6.2.2 Monthly Time Series

The next results, shown in Figure 6.9, are monthly time series of the calculated minus observed BT biases. Even with reduced sample numbers on the monthly scales, results for IASI -A and -B matchup datasets are qualitatively similar, with the only difference being the expected 0.1 K offset (not shown) between the IASI instruments. CrIS biases corresponding to Metop -A and -B have larger differences between themselves, with differences of up to 0.2 K (not shown)—likely due to insufficient sample numbers. Fig 6.9 specifically shows biases for IASI-B and GRAS-B for the five latitude zones and 3 different channels representing the ~35, 60, and 150 hPa pressure levels. For all levels, seasonal changes in the difference biases are larger in the SH and increase poleward. The tropical biases are overall constant with time and oscillate very slightly to be in and out of agreement across the 2 years of results. The extra-tropical biases are symmetric about the equator with positive maxima occurring during the winter solstices (NH: ~Dec 20th, SH: ~June 20th) and negative minima during the summer solstices. The dry biases have slightly more seasonal variation at higher levels in comparison to the wet/background biases, e.g. the Antarctic where the dry bias is ~0.5 K more negative than the wet/background biases in Nov and Dec 2015 at 35 and 60 hPa.

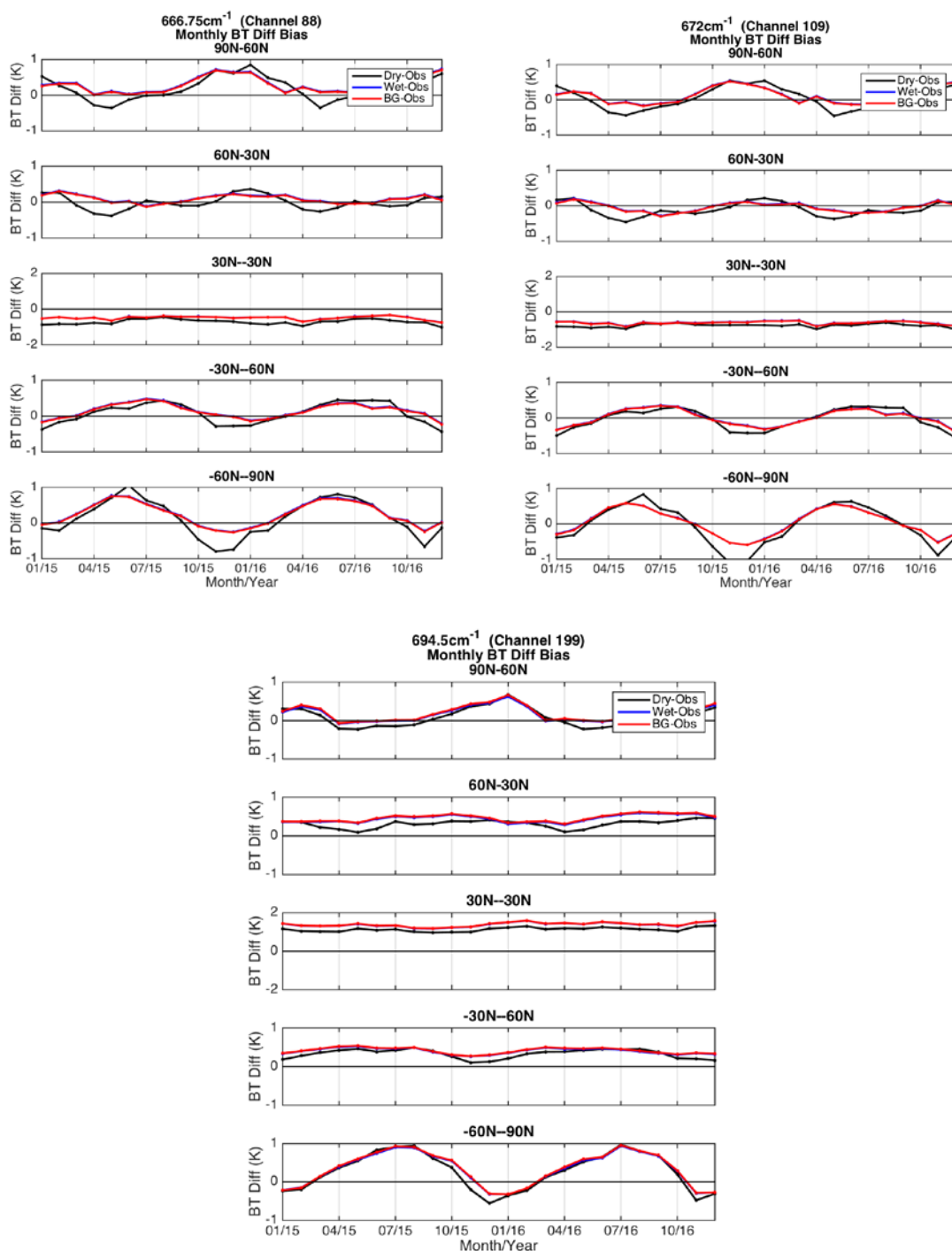


Figure 6.9 Monthly GRAS-B calculated minus IASI-B observed dry (black), wet (blue), and background (red) BT biases for 5 latitude zones for the ~35 hPa level (top left panels; IASI channel 88), ~60 hPa level (top right panels; IASI channel 109), and ~150 hPa level (bottom panels; IASI channel 199).

6.2.3 Solar Zenith Angle Dependence

To investigate possible dependencies on the solar zenith angle, Figures 6.10 and 6.11 show zonal BT biases for the 2015-2016 time frame for the ~30 and 150 hPa level respectively for 10° binned solar zenith angles. In the figures, both IASI-B/GRAS-B and CrIS/GRAS-B datasets overlaid. Due to the orbital mechanics and seasonal variations, results for all solar zenith angles are not available. Uncertainty of the biases (i.e. the standard deviation divided by the square root number of samples) are considered negligible for these analyses, being under 0.1 K, usually ~0.01 K.

For both levels, CrIS biases are overall qualitatively similar to the IASI biases, suggesting that the characteristics of the biases are more globally representative, rather than simply representing characteristics for the local sampling times of the IR sounder platforms. Differences between the dry and wet/background results are typically less than ~0.25 K with the dry bias generally more biased towards negative. For all pressure levels, the polar zones have biases which increase from negative to positive with increasing solar zenith angle so that all the dry, wet and background biases are warmer at nighttime. Seen more prominently at higher levels, the polar dry biases are farther from the wet/background biases for solar zenith angles less than ~90 degrees during the day—so that the dry and wet/background biases are more similar at night. For all levels, the tropical zone does not show any clear dependence on the solar zenith angle. The ~60 hPa results (not shown) show similar behaviors to the 30 and 150 hPa pressure level, suggesting a constant with height solar zenith angle dependence through the lower to middle stratosphere.

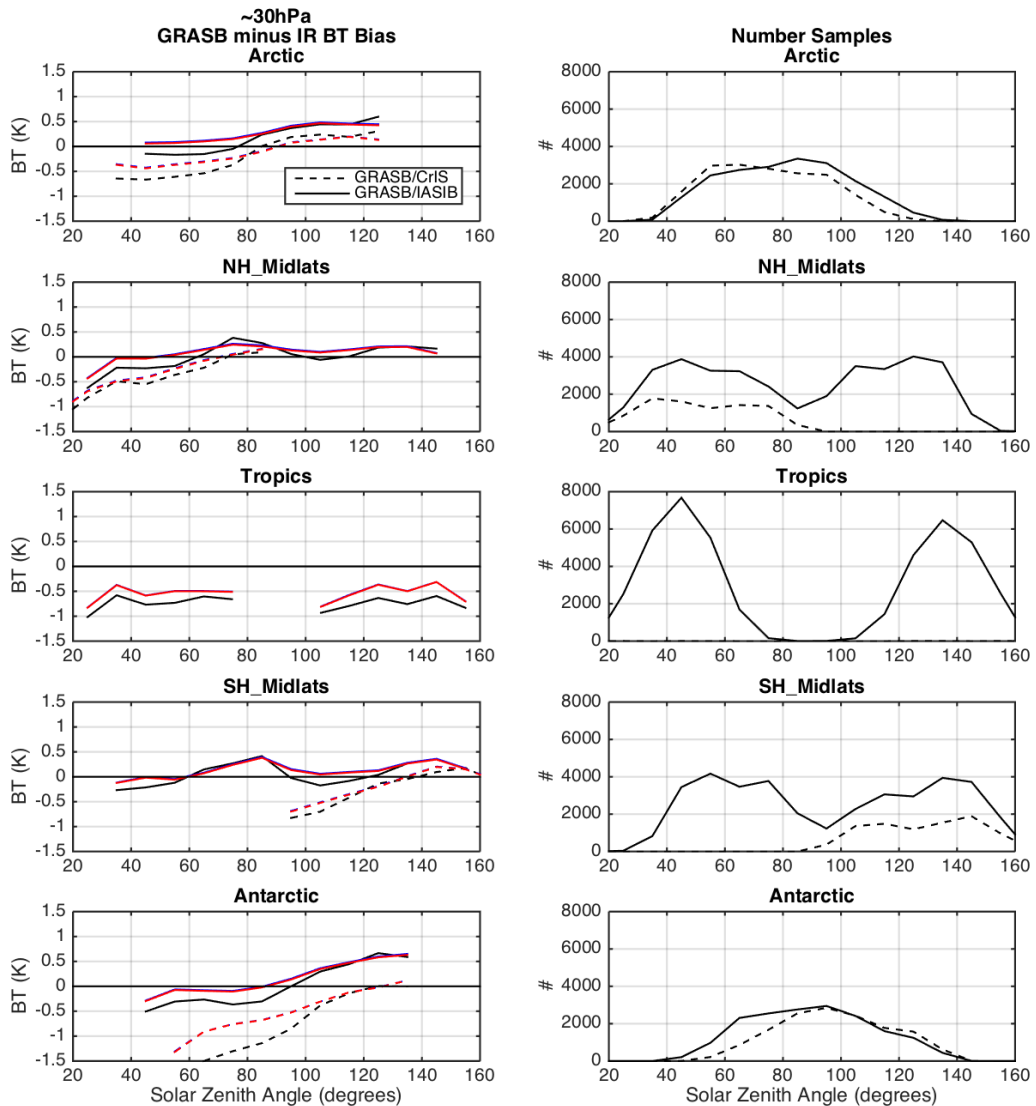


Figure 6.10 GRAS-B minus IASI-B (solid) and GRAS-B minus CrIS (dotted) ~30 hPa zonal BT biases (left) and number of samples (right) for 10 degree binned solar zenith angles over the Jan 2015 through Dec 2016 time period. Biases for the GRAS dry (black), wet (blue), and background (red) temperatures are overlaid. Solar zenith angles less than 90 degrees correspond to the sun being above the horizon.

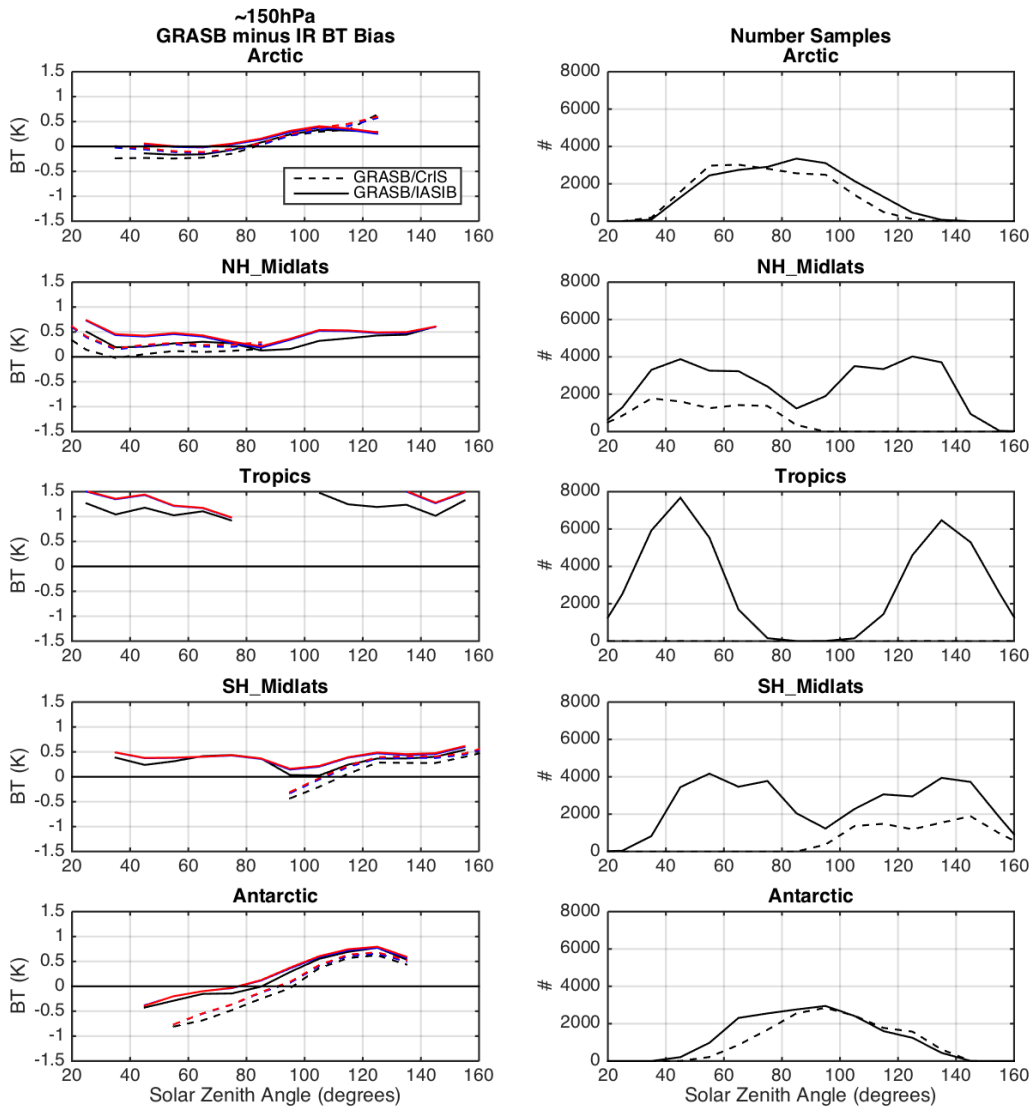


Figure 6.11 Same as Fig 6.9 except for ~150 hPa level.

7. Conclusions

7.1 Summary

Collocations of GRAS temperatures to IASI and CrIS radiances for the complete years of 2015-2016 using the <1 hour time criterion and coincident spatial selection allowed for an ample number of samples for the IASI/GRAS datasets on seasonal, zonal scales and for the CrIS/GRAS datasets in the extra-tropics on seasonal and 5 latitude bin scales. Analyses showed that the collocation datasets corresponding to the different Metop -A and -B platforms (i.e. IASIB/GRASB and IASIA/GRASA, etc.) had consistent BT difference biases, being generally within 0.1 K of each other. A simple, constant offset of ~0.1 K, known to be present between the IASI-A and -B hyperspectral IR sounders, was seen between the two IASI dataset biases. While CrIS and IASI datasets are not expected to be similar due to different orbital crossing times and WF shapes, they were within ~0.5 K of each other, generally less. For all collocation datasets, the wet and background BT difference biases were similar across all regions. Slight, up to 0.4 K temperature differences existed between the wet and background GRAS products in the UTLS; however, these were not seen in the BT biases likely due to the BT weighting function's shape, which averages over the higher vertical resolution differences between the wet and background temperatures.

An uncertainty for the calculated BTs was created using 4 assumed independent components which included an IR observation uncertainty, an RTM calculation uncertainty, an RO extrapolation uncertainty, and an RO temperature product error estimate. This uncertainty was used to represent stochastic errors. For channels of interest, the total calculated BT uncertainty estimate was ~0.55 K for the GRAS wet and background calculated BTs and ~0.7 up to ~1.2 K for the dry BTs. This total uncertainty estimate was compared to the GRAS calculated minus IR observed BT standard deviations. General agreement of the background/wet standard deviation with the BT uncertainty existed in mid-latitude and polar winter regions, while polar summers had smaller than expected background/wet standard deviations and tropical regions had larger than expected standard deviations. The dry standard deviations were larger than the BT uncertainty in all zones for channels with main contributions from pressure levels above (in altitude) the ~70 hPa level, indicating that the total BT uncertainty does not sufficiently account for the stochastic error sources. This was also seen in channels with contributions from pressure levels closer to the surface (100-300 hPa) in the JJA Antarctic zones.

Seasonal, zonal analyses and monthly time series showed variations of the bias with height were larger for the dry BT calculations than the wet and background—the dry biases tended to increase with height for altitudes above 100 hPa, contained more seasonal structure particularly at upper levels around ~30 hPa, and were farther from zero. Additionally, the calculated minus observed dry BT standard deviations tended to increase with height, being roughly ~0.5 K at 200 hPa and ~1.5 K at 30 hPa, in contrast to the relatively constant with height wet and background standard deviations which were constant with height and very roughly ~0.5 K. Tropical biases were seen to be overall constant with time. Extra-tropical biases contained seasonal structures, being symmetric about the equator with positive maxima occurring during the winter solstices (NH: ~Dec 20th, SH: ~June 20th) and negative minima during the summer solstices. These maxima in

the polar zones could be linked to the large horizontal temperature gradients which exist at the poles and pose a challenge to the RO temperature retrieval due to an assumption of spherical symmetry of the atmosphere.

An investigation of the solar zenith angle dependence of the statistics on annual, zonal scales for the ~30 and 150 hPa level showed CrIS biases were qualitatively similar to IASI biases. While the tropical zone biases did not have any clear dependence, the polar zones were characterized by biases which increased from negative to positive with increasing solar zenith angle so that the dry, wet and background biases were warmer when the sun was below the horizon. The dry product bias was typically more negative than the wet and background temperatures (by less than 0.25 K). Additionally, the polar dry biases were more similar to the dry and wet/background biases for solar zenith angles over 90 degrees—perhaps due to the lack of ‘water vapor contamination’ and ionospheric influences which would not be present in the background profiles and which would be corrected for in the wet product with the help of the background profiles.

7.2 Recommendations

This activity demonstrated a comparison of RO temperature products to hyperspectral IR sounder observations in brightness temperature space using uncertainty estimates. Though focused on the 15 micron region CO₂ absorption band which is sensitive to temperature in the 200 to 1 hPa range, this activity prompts consideration of a comparison of BT’s for all channels of the IR spectrum, which could provide other insightful comparison opportunities.

Recommendations include the investigation of regions which showed disagreements between the calculated minus observed BT standard deviations and the total BT uncertainty estimate. This includes the upper stratosphere (~70-10hPa) in all zones for the dry temperature, and it includes the polar summer and tropics for the wet/background temperature. Regions of relatively increased biases—specifically the polar regions around solstices and the lower stratospheric tropical region channels should also be investigated. Challenges in both the IR radiative transfer scheme and RO temperature derivation should be considered. Continued collaboration between the hyperspectral IR sounder and radio occultation communities could provide fruitful insights for both communities. Long term comparisons of RO temperatures and IR radiances could help confirm or refute trend results and diagnose potential characteristics in the data that are not due to characteristics of the measurand.

The presence of both hyperspectral IR sounders and RO receivers on the Metop satellite series platforms offers a unique opportunity to leverage the strengths of both the instruments to accomplish more than could be done with either one alone. Such collocation of instruments ensures that an ample number of samples is available for strict collocation requirements that ensure the comparisons are representative of similar temporal and spatial sampling. Such a large number of RO and IR sounder samples in coincident locations could potentially be fruitful for near real time validation in attempts to screen out extraneous measurements.

7.3 Acknowledgments

I would like to give a warm thanks to Johannes Nielsen at DMI for prompting the potential of such a visiting scientist study during his time at my home institute, and also for putting in the necessary work to see it through. Many thanks and kind regards are also given to Kent Lauritsen for being so hospitable during my time at DMI and supporting this activity, in addition to Stig Syndergaard and Hans Gleisner. All of them, including other members of the ROM SAF group, are appreciated for their friendly, fruitful, and encouraging discussions. I am grateful for my time with the ROM SAF group at DMI, which proved to be a very warm and friendly institute.

8. Appendix

8.1 BT Calculation Sensitivity Study

8.1.1 Constant Emissivity

For the RTM calculations, the input surface emissivity is set to be a constant ocean emissivity spectrum. The following analysis demonstrates why no error is expected to be introduced through this approximation for the channels analyzed in this study. Figure 8.1 illustrates a sensitivity test performed on the emissivity and skin temperature definition (skin temperature is strongly related to surface emissivity). Monochromatic BT spectra are computed using the reference Line-by-Line RTM for different definitions of these surface parameters which are varied independent of each other. Results shown in Figure 8.1 are the control minus perturbation BT spectra where the control emissivity is the ocean spectrum used in this study and the control skin temperature is an ersatz truth defined by the ERA reanalysis model. Results show that perturbations of up to 2.0 K in skin temperature and 0.02 in surface emissivity produce no noticeable change within the 650cm⁻¹ to 700 cm⁻¹ range which is used in this study, therefore, no uncertainty error is added to the BT calculations due to this approximation.

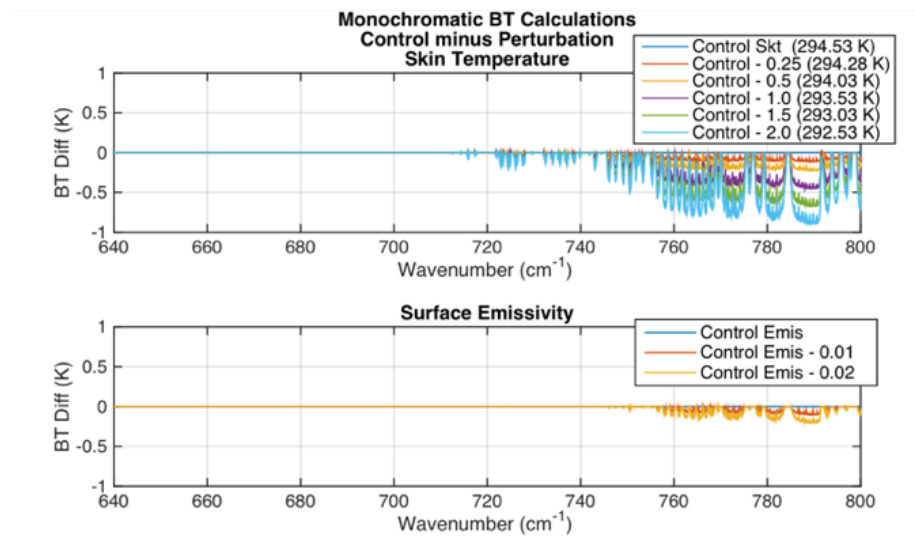


Figure 8.1 Sensitivity test of calculated BTs to the skin temperature (top panel) and surface emissivity (bottom panel) definition shown as perturbations from a control case which is defined as described in the text.

References

- Anderson, Gail P., S. A. Clough, F. X. Kneizys, J. H. Chetwynd, and E. Po Shettle. AFGL atmospheric constituent profiles (0.120 km). No. AFGL-TR-86-0110. AIR FORCE GEOPHYSICS LAB HANSCOM AFB MA, 1986.
- Aumann HH, Pagano TS. Using AIRS and IASI data to evaluate absolute radiometric accuracy and stability for climate applications. In: Goldberg MD et al., editors. Atmospheric and environmental remote sensing data processing and utilization IV: readiness for GEOSS II. International Society for Optical Engineering (SPIE Proceedings, vol. 7085); 2008. p. 708504. doi:10.1117/12.795225.
- Blumstein D, Tournier B, Cayla FR, Phulpin T, Fjortoft R, Buil C, et al. In-flight performance of the infrared atmospheric sounding interferometer (IASI) on METOP-A—art. no. 66840H. In: Goldberg MD, Bloom HJ, Huang AH, Ardanuy PE, editors. Atmospheric and environmental remote sensing data processing and utilization III: readiness for Geoss. Proceedings of the society of photo-optical instrumentation engineers (SPIE), vol. 6684. Bellingham: SPIE—International Society of Optical Engineering; 2007. p. H6840.
- Chou, M.-D., Weng, C.-H. & Lin, P.-H (Chou 2009). Analyses of FORMOSAT-3/COSMIC humidity retrievals and comparisons with AIRS retrievals and NCEP/NCAR reanalyses. *Journal of Geophysical Research-Atmospheres* 114, D00G03 (2009).
- Danzer, J., Foelsche, U., Scherllin-Pirscher, B. and Schwärz, M. Influence of changes in humidity on dry temperature in GPS RO climatologies, *Atmospheric Measurement Techniques*, 7, 2883–2896, doi:10.5194/amt-7-2883-2014.
- Dee, D. P., et al. (2011), The ERA-Interim reanalysis: Configuration and performance of the data assimilation system, *Quarterly Journal of the Royal Meteorological Society*, 137(656), 553-597.
- Divakarla, M., Barnet, et al. (Divakarla 2014). The CrIMSS EDR Algorithm: Characterization, optimization, and validation. *Journal of Geophysical Research: Atmospheres*, 119(8), 4953-4977.
- Feltz, M. L., Knuteson, R. O., Revercomb, H. E., and Tobin, D. C. (Feltz 2014a). A methodology for the validation of temperature profiles from hyperspectral infrared sounders using GPS radio occultation: Experience with AIRS and COSMIC, *Journal of Geophysical Research: Atmospheres*, 119, doi:10.1002/2013JD020853.
- Feltz, M., Knuteson, R., Ackerman, S. and Revercomb, H. (Feltz 2014b). Application of GPS radio occultation to the assessment of temperature profile retrievals from microwave and infrared sounders, *Atmospheric Measurement Techniques*, 7(11), 3751-3762, doi:10.5194/amt-7-3751-2014.
- Feltz, M., and R. Knuteson (Feltz 2014c). "Utility of a GPS Radio Occultation and Hyperspectral Infrared Sounder Matchup Dataset: Independent Comparisons." *Proceedings of the Eighth FORMOSAT-3/COSMIC Data Users' Workshop*. UCAR's Center Green Campus (CG1), Boulder, CO, USA. 2014. Poster.

- Feltz, M. L. , L. Borg, R. O. Knuteson, D. Tobin, H. Revercomb, and A. Gambacorta (Feltz 2017a). Assessment of NOAA NUCAPS Upper Air Temperature Profiles Using COSMIC GPS Radio Occultation and ARM Radiosondes, under review in JGR Atmospheres. UNDER REVIEW.
- Feltz, M. et al. (Feltz 2017b). Stratospheric Temperature Records: Multi-year assessment of COSMIC radio occultation and AIRS hyperspectral IR sounder products, accepted to JGR-Atmospheres. UNDER REVIEW.
- Goldberg, Mitchell D., and Hal J. Bloom. "Atmospheric and Environmental Remote Sensing Data Processing and Utilization V: Readiness for GEOSS III." Society of Photo-Optical Instrumentation Engineers (SPIE) Conference Series. Vol. 7456. 2009.
- Goldberg, M. D., H. Kilcoyne, H. Cikanek, A. Mehta (2013), Joint Polar Satellite System: The United States next generation civilian polar- orbiting environmental satellite system. *Journal of Geophysical Research: Atmospheres*, 118 (24).
- Han, Y., H. Revercomb, M. Crompton, D. Gu, D. Johnson, D. Mooney, ... and Y. Chen (2013), Suomi NPP CrIS measurements, sensor data record algorithm, calibration and validation activities, and record data quality, *Journal of Geophysical Research: Atmospheres*, 118(22).
- Hilton, F., R. Armante, T. August, C. Barnet, A. Bouchard, C. Camy-Peyret, ... and A. Collard (2012), Hyperspectral earth observation from IASI, *Bulletin of the American Meteorological Society*, 93(3), 347.
- Ho, S.-P., Kuo, Y.-H. & Sokolovskiy, S (Ho 2007). Improvement of the temperature and moisture retrievals in the lower troposphere using AIRS and GPS radio occultation measurements. *Journal of Atmospheric and Oceanic Technology* 24, 1726–1739 (2007).
- Illingworth, S. M., J. J. Remedios, and R. J. Parker. "Intercomparison of integrated IASI and AATSR calibrated radiances at 11 and 12 μm ." *Atmospheric Chemistry and Physics* 9.18 (2009): 6677-6683, DOI: 10.5194/acpd-9-8101-2009
- Isoz, O., Buehler, S.A., and Eriksson, P. (Isoz 2015). Intercalibration of microwave temperature sounders using radio occultation measurements, *J. Geophys. Res.*, 120, 3758- 3773, doi:10.1002/ 2014JD022699, 2015. Ladstädter, F (Ladstädter 2012). Collocating GRAS with nadir sounders onboard Metop: An assessment for instrument and climate monitoring. SAF/GRAS/DMI/REP/VS07/001 (available at: http://www.romsaf.org/visiting_scientist.php)
- Jouglet, D., et al. (2014), Radiometric and spectral inter-comparison of IASI: IASI-A/IASI-B, IASI/AIRS, IASI/CrIS, CALCON 2014 Meeting, Salt Lake City, UT, USA, 12 Aug 2014.
- Klaes, K. D., Cohen, M., Buehler, Y., and Schlüssel, P. (2007), An introduction to the EUMETSAT polar system, *Bulletin of the American Meteorological Society*, 88(7), 1085.
- Larar, A. M., et al. "IASI spectral radiance validation inter-comparisons: case study assessment from the JAIVEx field campaign." *Atmos. Chem. Phys* 10.2 (2010): 411-430, DOI: 10.5194/acp-10-411-2010.

- Liu, C.-Y. et al (Liu 2016). Retrieval of Atmospheric Thermodynamic State From Synergistic Use of Radio Occultation and Hyperspectral Infrared Radiances Observations. *Ieee Journal of Selected Topics in Applied Earth Observations and Remote Sensing* 9, 744– 756 (2016).
- Moncet, J-L., Uymin, G., Lipton, A. E., and Snell, H. E. (2008), Infrared radiance modeling by Optimal Spectral Sampling, *American Meteorological Society*, 65, 3917 - 3934, doi: 10.1175/2008JAS2711.1.
- Moncet, J-L., Uymin, G., Liang, P., and Lipton, A. (2015), Fast and accurate radiative transfer in the thermal regime by simultaneous optimal spectral sampling over all channels, *J. Atmos. Sci.*, 72, 2622-2641, doi: <http://dx.doi.org/10.1175/JAS-D-14-0190.1>.
- Newman, Stuart M., et al. "The joint airborne IASI validation experiment: an evaluation of instrument and algorithms." *Journal of Quantitative Spectroscopy and Radiative Transfer* 113.11 (2012): 1372-1390, <https://doi.org/10.1016/j.jqsrt.2012.02.030>
- Peters et al. (2007), An atmospheric perspective on North American carbon dioxide exchange: CarbonTracker, *PNAS*, 104(48), 18925-18930.
- Shi, Lei et al. (Shi 2016). Algorithm Development of Temperature and Humidity Profile Retrievals for Long-Term HIRS Observations, *Remote Sens.* 2016, 8(4), 280; doi:10.3390/rs8040280.
- Strow, L. L., et al. (2013), Spectral calibration and validation of the Cross-track Infrared Sounder on the Suomi NPP satellite, *Journal of Geophysical Research: Atmospheres*, 118(22).
- Tobin, D., et al. (2013), SuomiNPP CrIS radiometric calibration uncertainty, *Journal of Geophysical Research: Atmospheres*, 118(18).
- Wang, Likun, et al. "Comparison of AIRS and IASI radiances using GOES imagers as transfer radiometers toward climate data records." *Journal of Applied Meteorology and Climatology* 49.3 (2010): 478-492, <https://doi-org.ezproxy.library.wisc.edu/10.1175/2009JAMC2218.1>
- Wang, L., et al. "Radiometric consistency assessment of hyperspectral infrared sounders." *Atmos Meas Tech* 8 (2015): 4831-44, DOI: 10.5194/amtd-8-7161-2015
- Yunck, T. P., et al. (Yunck 2009), Use of radio occultation to evaluate atmospheric temperature data from spaceborne infrared sensors, *Terr. Atmos. Ocean. Sci.*, 20(1), 71-85, doi:10.3319/TAO.2007.12.08.01.
- Zavyalov, V., Esplin, M., Scott, D., Esplin, B., Bingham, G., Hoffman, E., Lietzke, C., Predina, J., Frain, R., Suwinski, L. and Han, Y., (2013), Noise performance of the CrIS instrument, *Journal of Geophysical Research: Atmospheres*, 118 (23).

List of Acronyms

AFGL	Air Force Geophysics Laboratory
BT	brightness temperature
COSMIC	Constellation Observing System for Meteorology, Ionosphere, and Climate
CrIS	Cross-Track Infrared Sounder
CT	Carbon Tracker
ECMWF	European Centre for Medium-range Weather Forecasts
EUMETSAT	European organisation for the exploitation of METeorological SATellites
GES DISC	Goddard Earth Sciences Data and Information Services Center
GNSS	Global Navigation Satellite System
GPS	Global Positioning System (USA)
GRAS	GNSS Receiver for Atmospheric Sounding (on Metop)
IASI	Infrared Atmospheric Sounding Interferometer
JPSS	Joint Polar Satellite System
Metop	Meteorological Operational Satellite
NetCDF	Network Common Data Form
NASA	National Aeronautics and Space Administration
NOAA	National Oceanic and Atmospheric Administration
NPP	National Polar-orbiting Partnership
NWP	Numerical Weather Prediction
OSS	Optimal Spectral Sampling
RO	Radio Occultation
ROM SAF	Radio Occultation Meteorology (ROM) Satellite Application Facility (SAF) (EUMETSAT)
RTM	Radiative transfer model
SIPS	Science Investigator-led Processing Systems
WF	Weighting Function